Neutrophils self-limit swarming to contain bacterial growth in vivo (#)

Korbinian Kienle[1,2,3], Katharina M. Glaser[1,2,3], Sarah Eickhoff[4], Michael Mihlan[1], Konrad Knöpper[4], Eduardo Reátegui[5,6], Maximilian W. Epple[1,2,3], Matthias Gunzer[7,8], Ralf Baumeister[9], Teresa K. Tarrant[10], Ronald N. Germain[11], Daniel Irimia[5], Wolfgang Kastenmüller[4], and Tim Lämmermann[1,*]

(#) This is the author's version of the work. It is posted here by permission of the AAAS for personal use, not for redistribution. The definitive version was published in *Science* 372 June 18, eabe7729, DOI: 10.1126/science.abe7729

Hyperlink: https://www.science.org/doi/10.1126/science.abe7729

Affiliations:

[1]Max Planck Institute of Immunobiology and Epigenetics, Freiburg, Germany.

[2]International Max Planck Research School for Immunobiology, Epigenetics and Metabolism (IMPRS-IEM), Freiburg, Germany.

[3]Faculty of Biology, University of Freiburg, Freiburg, Germany.

[4]Institute of Systems Immunology, University of Würzburg, Max Planck Research Group, Würzburg, Germany.

[5]Center for Engineering in Medicine, Massachusetts General Hospital, Harvard Medical School, Shriners Hospital for Children, Boston, MA, USA.

[6]William G. Lowrie Department of Chemical and Biomolecular Engineering, The Ohio State University, Columbus, Ohio, USA.

[7]Institute for Experimental Immunology and Imaging, University Hospital, University Duisburg-Essen, Essen, Germany.

[8]Leibniz-Institut für Analytische Wissenschaften - ISAS - e.V., Dortmund, Germany.

[9]Bioinformatics and Molecular Genetics, Faculty of Biology, Centre for Biochemistry and Molecular Cell Research, Faculty of Medicine, Signalling Research Centres BIOSS and CIBSS, University of Freiburg, Freiburg, Germany.

[10]Division of Rheumatology and Immunology, Department of Medicine, Duke University School of Medicine, Durham, NC, USA.

[11]Laboratory of Immune System Biology, National Institute of Allergy and Infectious Diseases, National Institutes of Health, Bethesda, MD, USA.

*Correspondence to: Tim Lämmermann (laemmermann@ie-freiburg.mpg.de)

Abstract

Neutrophils communicate with each other to form immune cell swarms in infected organs. Coordination of this population response is critical for the elimination of bacteria and fungi. We find that neutrophils have evolved an intrinsic mechanism to self-limit swarming and avoid uncontrolled aggregation during inflammation. G protein-coupled receptor (GPCR) desensitization acts as negative feedback control to stop migration of neutrophils when they sense high concentrations of self-secreted attractants that initially amplify swarming. Interference with this process allows neutrophils to scan larger tissue areas for microbes. Unexpectedly, this does not benefit bacterial clearance as the containment of proliferating bacteria by neutrophil clusters becomes impeded. Our data reveal how auto-signaling stops self-organized swarming behavior and how the finely tuned balance of neutrophil chemotaxis and arrest counteracts bacterial escape.

Introduction

The collective behavior of eukaryotic cells and insects is often based on self-organizing processes. The release of chemical signals, such as chemoattractants or pheromones, is one mechanism that allows individual entities to attract neighboring individuals, leading to the accumulation and aggregation of a whole population of cells or insects. Examples of such self-amplifying positive feedback control to initiate phases of self-organization include the collective defensive behavior of honeybees that attack hornets by thermo-balling (*1*), the aggregation behavior of locusts (*2*), and signal relay during the life cycle of *Dictyostelium* (*3*). However, the mechanisms that stop self-organization are poorly understood for many of these processes.

Neutrophils circulate in large numbers in the mammalian blood stream to patrol the body, thereby playing a central role in host defense (*4*). They exit blood vessels and infiltrate tissues to search for damaged cells and invading pathogens when the local surveillance by other tissue-resident immune cells fails to control inflammation or infection (*5, 6*). Therefore, neutrophil infiltrates and aggregates represent major histopathological hallmarks of acute tissue inflammation and infection. Intravital imaging in mouse tissues has revealed that collective-like swarming behavior underlies the formation of neutrophil aggregates in many mouse models of sterile tissue injury and infection with bacteria, fungi, and viruses (*7, 8*). During this population response, hundreds of individual neutrophils show coordinated sequential phases of highly directed chemotaxis, intercellular signal relay, and cluster formation. Reminiscent to the collective behavior of some insects and *Dictyostelium*, neutrophils self-amplify swarming in a feed-forward manner by secreting chemokines and chemoattractants, which allows intercellular communication and

provides the swarm a level of self-organization in the complexity of an inflammatory environment (*9*).

It remains unclear how this swarming response ceases to avoid uncontrolled neutrophil accumulation. The mechanisms for terminating this response in mammalian tissues have not yet been defined and may be controlled by external factors from the tissue environment or by neutrophils themselves, as suggested from simpler model systems (*10-12*). Based on our previous findings that neutrophils self-amplify swarming through the release of the chemoattractants leukotriene B4 (LTB4) and the chemokine C-X-C motif chemokine ligand 2 (CXCL2) (*9*), we hypothesized that the temporal local increase of these attractants causes the desensitization of the respective G protein-coupled receptors (GPCRs) (*13*), potentially acting as an internal feedback control for swarming neutrophils. It is well established that neutrophils can undergo GPCR desensitization and become unresponsive to repeated or continuous agonist stimulation in vitro (*14-16*). However, it remains unresolved if and how this process contributes to neutrophil navigation and swarming in mammalian tissues and, whether the anticipated desensitization plays a role in their physiological host defense functions.

Results

GRK2 controls GPCR desensitization and neutrophil arrest

We began our study of these issues by first examining whether active desensitization occurs during swarming. To this end, we interfered with GPCR desensitization by genetically targeting GPCR kinases (GRKs). These critical enzymes can phosphorylate cytoplasmic tails of an activated GPCR, which ultimately leads to the uncoupling of the GPCR from its signaling cascade and often GPCR internalization as well (*13*) (fig. S1A). As neutrophils express four GRK isoforms (GRK2, GRK3, GRK5, and GRK6) (*17-21*), we crossed several mouse strains to isolate

primary mature neutrophils that were efficiently depleted of individual GRKs or the complete GRK family (fig. S1, B to E). To identify the GRK isoforms that are functionally relevant for swarming, we imaged control and *Grk*-deficient neutrophils side-by-side in chemotaxis assays and analyzed their migratory response toward gradients of the primary swarm-mediating attractants LTB4 and CXCL2 (Fig. 1A). In these experiments, control neutrophils performed highly directed chemotaxis at the onset of the gradient before they slowed down, rounded up, and stopped migrating when reaching areas of high attractant concentrations (Fig. 1, B to D; fig. S1F; and Movie S1). Among all single *Grk*-deficient cells, only neutrophils lacking GRK2 (*Grk2*$^{-/-}$) displayed clearly distinct behavior. Previous work has shown that GRK2 in B and T cells selectively controls the desensitization of the GPCR sphingosine-1-phosphate receptor 1 (S1PR1), but not of several other lymphocyte-expressed GPCRs (*22*). In gradients of combined LTB4 and CXCL2, *Grk2*$^{-/-}$ neutrophils showed twice the displacement of control cells from the starting cell well (Fig. 1, A and B; and Movie S1). Maximum displacement of knockout cells ranged from 1.7–3.2 mm between independent experiments, whereas control cells reached 1–1.5 mm. At the onset of the gradient (early phase, 0–30 min), *Grk2*$^{-/-}$ neutrophils showed a slight increase in speed and *y*-straightness, a measure of chemotactic behavior, in comparison to control cells (Fig. 1C). However, the major effect of GRK2 depletion was observed in fields of high attractant concentrations (late phase, 90–180 min). *Grk2*$^{-/-}$ neutrophils did not arrest as did control cells, but they continued to move with polarized morphology at elevated speed (Fig. 1, D and E), before reaching an oscillating behavior with short alternating phases of forward and backward movement (fig. S1G). Similar motility behavior was observed in single gradients of LTB4 and CXCL2 alone (Fig. 1, F and G, and fig. S1G). We never observed net reverse migration of *Grk2*$^{-/-}$ cells. This persistent migration phenotype could not be attributed to gross alterations in the differentiation and maturation of control and *Grk2*$^{-/-}$ bone marrow neutrophils

(fig. S2A). Notably, the same GRK2-dependency was also evident with neutrophils isolated from blood (fig. S2, B and C), pre-activated neutrophils (fig. S2D), and wild-type (WT) neutrophils upon acute chemical GRK2 inhibition (fig. S2E). Depletion of all four GRK isoforms in neutrophils (4×*Grk*$^{-/-}$) did not additionally increase the migratory response in LTB4/CXCL2 gradients (Fig. 1A; fig. S2F; and Movie S1), highlighting the major role of GRK2 in this process. Importantly, *Grk2*$^{-/-}$ neutrophils did not show this substantial increase in responsiveness for all GPCR ligands known to attract neutrophils. When comparing the displacement of *Grk2*$^{-/-}$ relative to control neutrophils in gradients of attractants binding to formyl peptide receptors (FPR1 and FPR2) or the complement component 5a anaphylatoxin chemotactic receptor 1 (C5aR1), which are GPCRs that do not show an important role during neutrophil swarming to modest sterile injury (*9*), we could only measure minimal or statistically non-significant differences (Fig. 1F). These findings indicated a particular role for GRK2 in controlling GPCRs that sense neutrophil-secreted LTB4 and CXCL2 and contribute to the self-amplification of neutrophil swarming. As GRK2 can also act on non-GPCR substrates (*23*), we directly tested GPCR desensitization by exposing neutrophils to repeated stimulation with increasing concentrations of agonist and measured the transient increase in intracellular calcium as a read-out for cellular responsiveness. Control neutrophils became unresponsive upon sequential stimulation, whereas *Grk2*$^{-/-}$ neutrophils remained responsive to a third GPCR activation through LTB4 or CXCL2 (Fig. 1, H and I). As a consequence, *Grk2*$^{-/-}$ neutrophils showed increased activation of pro-migratory mitogen-activated protein kinase (MAPK) signaling cascades downstream of GPCR activation when we activated cells with the same triple rising stimulation that was used in the calcium-flux assay (fig. S3, A and B). Notably, repeated stimulation of control and *Grk2*$^{-/-}$ neutrophils with the attractant complement component 5a (C5a) did not produce any differences in calcium and MAPK signaling measurements (fig. S3C).

To test the effect of GPCR desensitization on neutrophil movement, we pre-treated control and *Grk2*$^{-/-}$ cells with concentrations of LTB4 and CXCL2 that caused receptor desensitization in the calcium-flux assay, before analyzing GPCR-mediated chemokinesis. In agreement with our results on GPCR desensitization in calcium and MAPK signaling measurements, ligand-pretreated *Grk2*$^{-/-}$ cells were more chemokinetic than control cells for both LTB4 (fig. S3D) and CXCL2 (fig. S3, E and F) which was reflected by increased speed and track lengths. Lastly, we tested if GRK2-controlled desensitization is accompanied by receptor internalization. In agreement with previous reports that found little if any internalization of the LTB4 receptor 1 (LTB4R1) (*24-26*), we did not observe any reduction in cell surface expression of this receptor in WT and *Grk2*$^{-/-}$ cells upon exposure to high concentrations of LTB4 (fig. S3G). There was a time-dependent decrease in cell surface expression of the C-X-C motif chemokine receptor 2 (CXCR2) in both WT and *Grk2*$^{-/-}$ neutrophils, in agreement with previous reports (*26*). However, cell surface levels of CXCR2 remained substantially higher in *Grk2*$^{-/-}$ neutrophils (fig. S3H). Thus, GRK2 plays a crucial role in attenuating GPCR activation with swarm-mediating attractants, which maintains neutrophil motility in fields of high attractant concentrations.

Neutrophils and eosinophils self-limit swarming

Neutrophil swarms come in a range of phenotypes and can be categorized into persistent and transient swarms (*7*). Persistent swarms show sustained neutrophil recruitment to form large cell clusters that can remain stable for hours, whereas transient swarms form smaller clusters that last only for minutes before neutrophils leave the aggregate and join nearby competing swarms. To investigate the role of GPCR desensitization for persistent swarm dynamics, we first employed large microscale arrays of fluorescent heat-killed bioparticle clusters, a previously established experimental system to analyze neutrophil swarming in vitro (*12*). Upon exposure to 400-µm-

spaced micropatterns of heat-killed *Staphylococcus aureus* (HKSA), sentinel neutrophils sensed the bioparticles and induced a recruitment wave of following neutrophils, which then formed cell clusters in a LTB4- and CXCL2-dependent manner (*12*) (Fig. 2A and fig. S4, A and B). In experiments with 1:1 mixtures of differentially dye-labeled control and *Grk2*$^{-/-}$ cells, we quantified neutrophil aggregation behavior in competitive clusters (fig. S4C). The accumulation index (AI), which is the ratio of *Grk2*$^{-/-}$ signal to WT signal on HKSA spots, was used as a measure of neutrophil aggregation. Strikingly, *Grk2*$^{-/-}$ neutrophils showed pronounced aggregation and dominated over control cells in competitive clusters, a behavior that was reflected in a mean AI value >1 (Fig. 2B and fig. S4C). By comparison, competitive clusters of two populations of control cells resulted in a mean AI=1 (Fig. 2B). Next, we examined the role of GRK2 in regulating persistent swarms in vivo by using an inducible model of sterile skin injury in which a brief laser pulse causes focal, dermis-restricted tissue damage (*9*). After intradermal co-injection of differentially dye-labeled control and *Grk2*$^{-/-}$ neutrophils, we used two-photon intravital microscopy (2P-IVM) to image the swarming response of the transferred cells to the induced skin wound for 1–1.5 hours (Fig. 2C and fig. S5A). Neutrophils that swarmed from the surrounding tissue toward the site of injury were tracked and migration parameters analyzed (Fig. 2D and fig. S5B). Control and *Grk2*$^{-/-}$ neutrophils were recruited at comparable speed and straightness toward the injury site (Fig. 2E; fig. S5C; and Movie S2), demonstrating that the minor measured effect on early-phase chemotaxis in vitro was not relevant for migration in native tissue (Fig. 1C). We then analyzed the ensuing step of the swarming response, swarm aggregation. To quantify neutrophil clustering in the skin, we defined the AI as a measure of cell entry into the collagen-free zone, as previously described (*9*). In our previous study (*9*), we only identified gene knockouts that showed impaired neutrophil aggregation behavior and mean AI values <1. Remarkably, *Grk2*$^{-/-}$ neutrophils gravitated more than WT cells toward the central

region of large competitive clusters, resulting in mean AI values >1 (Fig. 2, F to H, and fig. S5D). Improved aggregation behavior of *Grk2*$^{-/-}$ cells was also observed in experimental set-ups that allowed the analysis of small clusters (fig. S5E and Movie S2). In contrast to control cells, *Grk2*$^{-/-}$ neutrophils remained actively motile in a growing cluster and continued to move toward the cluster center where they outcompeted WT cells over time (Fig. 2G; fig. S5D; and Movie S2). GRK3, GRK5, or GRK6 deficiency had no measurable effect on central accumulation (Fig. 2H and fig. S5F). Finally, we also studied persistent swarms of eosinophils, another innate immune cell type, that self-amplify their collective migration response to worms by paracrine LTB4 signaling (*27*). Like neutrophils, swarming *Grk2*$^{-/-}$ eosinophils aggregated more closely than WT cells around *Caenorhabditis elegans* larvae (Fig. 2I; fig. S5G; and Movie S2), confirming the more general role for GRK2 in swarming responses beyond neutrophil biology. Thus, GRK2 acts as negative regulator of swarming in mammalian tissues and GPCR desensitization is integral at sites where swarming granulocytes accumulate and self-generate a local field of high attractant concentrations.

Increased tissue scanning is not beneficial for bacterial elimination

In many inflammatory conditions, neutrophils respond to cell death at multiple locations within a tissue, leading to several transient swarms whose attractant release influences the growth and disappearance of each other (*7*). To address the role of GRK2 in situations where migrating neutrophils sense multiple attractant sources, we pre-exposed WT and *Grk2*$^{-/-}$ neutrophils to LTB4/CXCL2 before they moved along a gradient of both agonists. In agreement with our calcium measurements (Fig. 1, H and I), WT neutrophils desensitized and became unresponsive to the subsequent attractant gradient in a concentration-dependent manner. By contrast, *Grk2*$^{-/-}$ neutrophils remained responsive at high attractant concentrations and could still move along the

gradient of activating signals (fig. S6A). Next, we analyzed the sequential navigation behavior of neutrophils in the presence of two spatiotemporally separated gradients of swarm attractants (Fig. 3A) (*28*). As observed previously (Fig. 1, A to D), *Grk2*$^{-/-}$ neutrophils migrated significantly more than control cells toward an initial source of LTB4/CXCL2. Importantly, *Grk2*$^{-/-}$ neutrophils were redirected by an additional second gradient at 90° angle, whereas control cells were not (Fig. 3A; fig. S6, B and C; and Movie S3). Thus, neutrophils lacking GRK2-mediated GPCR desensitization increase their space exploration between competing gradients of swarm attractants.

To gain insight into the possible in vivo relevance of our findings, we investigated the role of GRK2 during transient neutrophil swarming in lymph nodes infected with *Pseudomonas aeruginosa* or *Salmonella typhimurium*. We have previously shown that several bacteria species induce cell death in subcapsular sinus (SCS) macrophages, subsequently leading to neutrophil recruitment and swarming in lymph nodes (*9, 29*) (Fig. 3B). Neutrophil depletion in these infection models leads to a substantial increase of bacteria growth in lymph nodes (*29*). By imaging endogenous WT and *Grk2*$^{-/-}$ neutrophils in SCS of mixed bone marrow chimera, we found again that knockout cells dominated over control cells in the central regions of newly forming clusters (Fig. 3, C and D; fig. S6, D and E; and Movie S3). This was reflected in AI values >1 (Fig. 3D). Moreover, *Grk2*$^{-/-}$ neutrophils moved faster than WT cells between clusters and explored larger tissue areas (Fig. 3E; fig. S6F; and Movie S3). Such behavior may be linked to more effective bacterial sampling throughout the infected organ, leading us to undertake a quantitative assessment of how GRK2 deficiency in neutrophils impacts bacterial clearance. The draining lymph nodes of mice with neutrophil-specific depletion of GRK2 (*Mrp8Cre Grk2*$^{fl/fl}$, "*Grk2*$^{\Delta PMN}$") and controls were analyzed following subcutaneous infection with *P. aeruginosa*.

To our surprise, there were significantly higher bacterial counts in the lymph nodes of *Grk2*$^{\Delta PMN}$ mice compared with control mice (Fig. 3F), although neutrophil recruitment into infected lymph nodes was comparable (fig. S6G). Thus, an inverse relationship exists between persistent neutrophil interstitial movement and bacterial elimination.

GPCR-controlled neutrophil arrest is critical for restricting bacterial growth

To understand in detail how GRK2-controlled neutrophil swarming counteracts bacterial growth, we established an experimental in vitro mimic of a bacteria-infected SCS. By co-culturing macrophages, neutrophils, and *P. aeruginosa* bacteria, we were able to follow the dynamics and major cellular events of SCS components with live-cell microscopy (Fig. 4A). In this system, bacteria performed pack swarming and invasion of macrophages (*30*), causing cell death as previously shown in vivo (*29*) (fig. S7, A to C, and Movie S4). Neutrophils showed swarming behavior and formed prominent clusters around locally proliferating bacteria and dying cells (Fig. 4B and fig. S7D). In agreement with our in vivo findings, *Grk2*$^{-/-}$ neutrophils dominated over control cells in cluster centers in competitive experiments (fig. S7E). When control and knockout cells were studied individually, *Grk2*$^{-/-}$ cells formed larger neutrophil aggregates around bacterial clusters than WT cells (Fig. 4C and Movie S4). However, GRK2-deficiency resulted in higher counts of "free" bacteria outside of neutrophil clusters and a significant increase of bacterial growth (Fig. 4C), confirming the results of our mouse infection model. This could not be attributed to changes in neutrophil maturation or major effector functions, as *Grk2*$^{-/-}$ and control cells were comparable in standard phagocytosis assays (HKSA and living *P. aeruginosa*) and in their release of reactive oxygen species, neutrophil elastase, and myeloperoxidase (fig. S8, A to E). We also only rarely observed neutrophil extracellular traps (NETs) around the small bacteria aggregates in our co-culture system and depletion of GRK2 had no measurable effect on

NET formation (fig. S8F), a process that has previously been reported to occur in the presence of *P. aeruginosa* biofilms (*31*). Establishing single-cell tracking of neutrophils in clusters helped identify the GRK2-regulated cellular mechanism limiting bacterial growth. Control cells slowed down their persistent migration and stopped in cell aggregates, whereas many *Grk2*$^{-/-}$ neutrophils lacked such arrest phases and migrated at high speed out of clusters again (Fig. 4, D to F; fig. S7F; and Movie S4). This uncontrolled persistent movement of *Grk2*$^{-/-}$ neutrophils had two functional consequences. First, knockout cells were impaired in picking up and ingesting microbes from bacteria clusters (Fig. 4G). Second, *Grk2*$^{-/-}$ cells were often unable to completely contain locally proliferating bacteria, allowing a breach in the swarm-dependent barrier and subsequent pathogen escape (Fig. 4H). Thus, GRK2-controlled neutrophil arrest is critical for bacterial phagocytosis and containment in swarm clusters. These findings emphasize that neutrophils have evolved a cell-intrinsic mechanism that self-limits dynamic cell behavior within forming swarms and ensures optimal elimination of bacteria (figs. S9 and S10).

Discussion

Neutrophil navigation through inflamed and infected tissues has long been viewed from a single-cell perspective, where cells were considered individually guided by external signals released from the tissue environment or directly from pathogens. It is now clear that neutrophils auto-signal to initiate a self-amplified population response, which accumulates these cells in large numbers and concentrates their effector functions at sites of damaged tissue or pathogen invasion (*7, 9*). Here we describe a cell-intrinsic stop mechanism for the self-organization of collective behavior, which is based on sensing the local accumulation of the same cell-secreted attractants that amplify swarming during early stages. Our findings highlight a crucial role of GPCR desensitization in attenuating the self-organized swarming dynamics of neutrophils in

mammalian tissues (fig. S9). When neutrophils sense high concentrations of swarm-secreted attractants (LTB4 and CXCL2), as found in growing neutrophil clusters, the GPCR-kinase GRK2 desensitizes the corresponding GPCRs to induce migration arrest. As GRK2 has only minimal effects on the desensitization of GPCRs that detect tissue- or bacteria-derived attractants (e.g., N-formyl peptides and C5a), neutrophils in swarm aggregates remain responsive to new tissue insults. This allows their redirection from neutrophil clusters to novel sites of cell death in tissues. Thus, our findings agree with earlier in vitro studies which highlighted the capacity of "end-target" attractants (N-formyl peptides and C5a) to override "intermediary" attractants (LTB4, CXCL2) and redirecting neutrophils out of "intermediary" attractant fields (*28, 32*). The described GRK2-mediated feedback control to swarm attractants is particularly critical in infected tissues, where it fine-tunes the local migratory arrest of neutrophils for optimal containment of proliferating bacteria (fig. S10). This provides a potential mechanistic explanation for earlier studies that implicated neutrophil swarming in restricting microbial growth in vitro (*33*) and in vivo *(34)*. Although we identified GRK2 as a key molecular brake on GPCR activation by neutrophil swarm attractants, its function may extend to other GPCRs in different inflammatory settings (*35, 36*).

How migrating phagocytes coordinate cell movement and phagocytosis and negotiate these two actin-dependent processes has been intensely studied in other phagocytic cells, including dendritic cells, *Dictyostelium*, and *Drosophila* macrophages (*37-43*). Most of these studies were performed in vitro or in simpler model organisms and focused on the analysis of individual cells and their uptake of inert elements. We here addressed the population dynamics of phagocytes and how these cells coordinate stop-and-go behavior within the population by self-secreting attractants. We define a cell-intrinsic, GPCR-based mechanism for stopping the swarming behavior of neutrophils, which is functionally relevant for the containment of proliferating living

bacteria in infected mammalian tissues. This described self-limiting mechanism does not rely on adaptations in gene regulation as commonly found in the bacterial population responses of quorum sensing and quenching (*44*). Local attractant degradation and the release of pro-resolving mediators are other potential self-limiting processes that emerged from in vitro studies (*12, 45*). However, it is still unclear if these processes also contribute to neutrophil swarming in tissues and augment the mechanism described herein.

These findings provide insights into the navigation strategies employed by neutrophil populations for the optimal elimination of bacteria in infected mammalian tissues. This should prove useful for an integrated view of self-limiting processes and active anti-inflammatory programs in controlling the resolution of neutrophil swarms, which is a critical step for tissue repair following infection. Our results also highlight the fact that desensitization to a self-produced activation signal acts as an important biological principle of self-organization, which is likely relevant for other forms of collective behavior in cells and insects.

Materials and Methods:

Mice

Table S1 in the Supplementary Material lists all mouse strains and crosses used in this study. *Mrp8-Cre* (*46*), *Grk2*$^{fl/fl}$ (*47*), *Grk3*$^{-/-}$ (*48*), *Grk5*$^{fl/fl}$ (*49*), *Grk6*$^{fl/fl}$ (*50*), *Lyz2*^{gfp} (*51*), *Ly6g*$^{cre/+}$ *Rosa26*$^{LSL:Tom}$ (*52*), *Vav-iCre* (*53*), *CAG-DsRed* (*54*), *Tyr*$^{c\text{-}2J/c\text{-}2J}$ (B6.Albino) (*55, 56*) and Lifeact-GFP (*57*) mouse strains have been described elsewhere. Mice were maintained in specific-pathogen-free conditions at an Association for Assessment and Accreditation of Laboratory Animal Care-accredited animal facility at the NIAID (NIH) and in a conventional animal facility at the Max Planck Institute of Immunobiology and Epigenetics according to local regulations. Mice were used for experiments at 8–16 weeks of age. Mice were age- and sex-matched in all experiments and littermate animals were used as controls in most experiments. All animal procedures were performed according to study protocols approved by the German authorities and the Regional Council of Freiburg, the Animal Care Commission of the state of North Rhine-Westphalia (LUA NRW) and the NIAID Animal Care and Use Committee (NIH), respectively.

Neutrophil isolation and labeling

For all in vitro experiments, mouse neutrophils were isolated from bone marrow (tibiae, femora, and os coxae) or peripheral blood using autoMACS® Pro Selector cell separator and MACS Neutrophil Isolation Kit for negative selection according to the manufacturer's protocol (Miltenyi Biotec). For intradermal injection experiments, mouse neutrophils were isolated from bone marrow using a three-layer Percoll gradient of 78%, 69%, and 52% as previously described (*9*). Neutrophil purity was >95% for both isolation procedures, as indicated by Ly6G^{+} phenotype in flow cytometry. When neutrophils required fluorescent cell labeling in subsequent experiments, they were incubated for 25 min at 2×10^{7} cells/ml with 0.5 µM CellTracker™ Green (CMFDA), 10 µM CellTracker™ Blue (CMF_2HC), 1 µM CellTracker™ Deep Red, or 10 µM 5-carboxytetramethylrhodamine, succinimidyl ester (5-TAMRA SE) in 1X PBS supplemented with 0.0002% (w/v) pluronic F-127 (all Thermo Fisher), as indicated for each experiment. After labeling, neutrophils were washed three times with 2% fetal bovine serum (FBS) and 2 mM EDTA in HBSS. In most experiments, neutrophils isolated from bone marrow were used, if not otherwise indicated.

Neutrophil chemotaxis and navigation assays

To analyze GPCR-driven neutrophil migration toward increasing concentrations of chemoattractants, we used under-agarose chemotaxis assays with slight modifications to the standard protocol (*58*). Agarose gels were cast into 35×10-mm tissue culture dishes (Corning). After gel polymerization, wells with a diameter of 4 mm were punched into the gel in approximately 3-mm distances using a template. Unless stated otherwise, five wells were punched in the agarose gel per dish: one central well for the chemoattractant surrounded by four equidistant wells for the cells. For side-by-side comparisons of control and gene-deficient neutrophils, cells were differentially labeled with CellTracker™ Green and 5-TAMRA SE. Neutrophils isolated from a pair of GRK-deficient and control mice were used for an independent experiment. Four technical replicates were performed in one independent experiment: two replicates with one dye combination, the other two replicates with interchanged dyes between control and gene-deficient neutrophils to exclude unspecific effects. Data analysis is described in the relevant methods section below. For triple comparisons of WT, *Grk2*$^{-/-}$, and 4×*Grk*$^{-/-}$

neutrophils, the third neutrophil population was labeled with CellTracker™ Blue. The outer four wells in the agarose gel were loaded with 20 µl of control and GRK-deficient neutrophils at a ratio of 1:1 (double comparison) or 1:1:1 (triple comparison) to obtain 1×10^5 cells in 10% FBS and 2 mM L-glutamine in phenol-free RPMI. The central well was loaded with 20 µl of chemoattractant at the following concentrations, if not indicated otherwise: 1 µM LTB4 (Cayman) and 1 µM murine CXCL2 (PeproTech), 1 µM LTB4 alone, 1 µM murine CXCL2 alone, 10 µM WKYMVM (Tocris), 1 µM WKYMVm (Tocris), or 1 µM murine C5a (PeproTech). For chemotaxis experiments referred to as "FPR1 stim", the FPR1/FPR2 selective chemoattractant WKYMVm was used in the presence of the selective FPR2 inhibitor WRW4 (100 µM, Tocris). Experiments with the selective FPR2 chemoattractant WKYMVM were referred to as "FPR2 stim". To acutely inhibit GRK2 function in control neutrophils, cell chemotaxis was performed in the presence of 30 µM CMPD101 (HelloBio). For every inhibitor treatment, cells were first pre-incubated with the inhibitor for 30 min at 37°C and then directly transferred to the wells without inhibitor washout. For neutrophil pre-activation, 50 ng/ml of TNF-α was added to the cells for 10 min before loading. To mimic the activation that neutrophils undergo upon extravasation into an inflamed tissue (*59*), cells were pre-incubated in a Lab-Tek (Thermo Fisher/Nunc) coated with 10 µg/ml of murine CXCL1 (KC) (PeproTech), 8 µg/ml of ICAM-1, and 2 µg/ml of PECAM-1 (both R&D Systems) for 1 hour before transfer to the chemotaxis dish. To analyze sequential navigation behavior, neutrophils were exposed to a first gradient of LTB4/CXCL2 (0.5 µM each), before adding 3 hours later a second gradient of LTB4/CXCL2 (1 µM each) at a 90° angle. For pre-incubation experiments, neutrophils were pre-incubated with LTB4/CXCL2 (0.1 µM or 1 µM each) for 30 min before chemoattractants were washed out and cells subsequently loaded into the wells of the under-agarose assay. Neutrophil migration was followed for 4 hours at 37°C. Cell migration underneath the agarose gel in direction to the gradient was recorded. Images were acquired for each well with a spinning-disk confocal microscope (Carl Zeiss Microimaging) at 10X magnification using multiple tiles to capture the whole well including all cells that left the well. Live-video microscopy was performed using a confocal spinning-disk microscope equipped with a stage-top incubator (TokaiHit) to generate an ambient atmosphere of 37°C and 5% CO_2. For confocal spinning-disk microscopy, we used a Cell Observer SD system (Carl Zeiss) comprising CSU-X1 confocal scanner unit (Yokogawa) mounted on an AxioObserver Z1 inverted microscope stand, and equipped with Evolve back-illuminated EM-CCD camera (Teledyne Photometrics). Depending on the used fluorochromes, images were acquired using laser-line excitation by 488 nm, 561 nm, 405 nm, or 639 nm solid-state lasers. A Plan-Apochromat 10X 0.45 objective and multiple-tiles function in ZEN software were used for image acquisition during live-cell imaging experiments and for experiments with endpoint analysis.

Neutrophil swarming on micropatterns

Microscale arrays of bioparticle clusters were manufactured as previously described (*12*). For pattern design, heat-killed *Staphylococcus aureus* (SA) Texas Red particle conjugates (Sigma-Aldrich) were used. The slides had an eight-well table format consisting of 10 patterns per row arranged in eight columns with single pattern diameters of 130 µm. Before neutrophils were added, wells were coated with 10% SA-opsonization reagent (Thermo Fisher Scientific) and 10 µg/ml fibronectin in FBS for 1 hour followed by three washes with 1X PBS. Control and GRK2-depleted neutrophils were differentially labeled with CellTracker™ Green and 5-TAMRA SE, mixed 1:1 and pre-activated with 50 ng/ml TNF-α (PeproTech) for 10 min. Neutrophils were then suspended in bovine collagen I (Nutacon) at a final gel concentration of 1 mg/ml and a density of

2×10^6 cells/ml, before 180 µl of the neutrophil–gel suspension was added to each well. To inhibit leukotriene biosynthesis, neutrophils were pre-incubated with 10 µM MK-886 (5-lipoxygenase-activating protein inhibitor, Calbiochem) for 30 min. To inhibit CXCL2 signaling, neutrophils were pre-incubated with 50 µM SB225002 (CXCR2 antagonist, Tocris) for 30 min. Loaded slides were incubated for 2-3 hours at 37°C before image acquisition. Images of whole slides were acquired at 10X magnification using the confocal spinning-disk microscope system as described in the section "Neutrophil chemotaxis".

Eosinophil swarming assay

Eosinophils were obtained from a murine bone marrow culture according to a reported protocol (*60*). In brief, cultures of bone marrow cells were first supplemented with 100 ng/ml SCF and 100 ng/ml FLT3-L (PeproTech) for 4 days. On day 4, the medium was replaced with medium containing 10 ng/ml of murine IL-5 (PeproTech). Every second day, one half of the medium was replaced by medium containing fresh IL-5 until eosinophils were ready to use on day 14. Eosinophil maturation was checked by Siglec-F expression using flow cytometry (>99% Siglec-F^+ cells at day 14). Bone marrow of *Vav-iCre Grk2$^{fl/fl}$* mice was used to deplete GRK2 in eosinophils. Four-day-old *Caenorhabditis elegans* dauer larvae carrying the *daf-2 (e1370)* allele were prepared by growing the worms at 25°C using standard methods, and kindly provided by R. Baumeister (University of Freiburg, Germany). Eosinophil swarming in response to nematodes in a 3D in vitro system has previously been described (*27*). Briefly, nematodes were suspended at a concentration of 6000 larvae/ml in Matrigel (Corning). Control and gene-deficient eosinophils were differentially labeled with CellTracker™ green and 5-TAMRA, SE, and mixed 1:1 at a concentration of 3×10^6 cells/ml. Eosinophils in medium were mixed with nematodes in Matrigel at a 1:1 ratio and added into eight-well Lab-Tek imaging chambers. After 2 hours incubation, images of single nematodes were acquired. Live-video microscopy was performed using a spinning-disk confocal microscope equipped with a stage-top incubator to generate an ambient atmosphere of 37°C and 5% CO_2. For time-lapse videos, an LD LCI Plan-Apochromat 25X/0.8 Imm objective (Zeiss) was used and images were acquired every minute for 2 hours. For quantitative analysis, single images of individual nematodes with clusters of eosinophils were acquired after 2 hours at 10X magnification using the confocal spinning-disk microscope system as described in the section "Neutrophil chemotaxis".

Neutrophil GPCR desensitization: Calcium-flux analysis

To analyze GPCR desensitization in response to increasing concentration of chemoattractant, transient increases of intracellular calcium (Ca^{2+}) in neutrophils were measured by flow cytometry. Neutrophils isolated from bone marrow were loaded with 2 µg/ml of Indo-1 AM according to the manufacturer's instructions (Thermo Fisher Scientific). In brief, ratiometric changes in intracellular calcium flow were measured using LSRIII flow cytometer (BD Biosciences) equipped with a sample heater at 37°C. Before acquisition, neutrophils were prewarmed in a water bath at 37°C for 10 min. During acquisition, neutrophils were maintained in a sample heater at 37°C and only removed shortly for stimulant addition. At the beginning of experiments, a 30-s baseline was recorded. Then, cells were stimulated at t=0.5 min, t=4 min, and t=8 min, and real-time intracellular Ca^{2+}-flux was recorded. Recording was stopped at t=10 min. Cells were stimulated with increasing concentrations of LTB4 (50 nM, 100 nM, and 200 nM) (Fig. 1H), CXCL2 (50 nM, 100 nM, and 200 nM) (Fig. 1I), CXCL2 (10 nM, 20 nM, and 40 nM) (fig. S3F), or C5a (5 nM, 10 nM, and 20 nM) (fig. S3C). To quantify receptor desensitization upon multiple stimulations, the area under the curve (AUC) (0-100 s after each stimulation) of

the Ca^{2+} flux was measured using FlowJo software. Desensitization was measured as the ratio of the AUC of the second or third stimulation to the AUC of the first stimulation in each independent experiment. In rare cases, experiments were excluded from analysis when neutrophils did not display detectable calcium signals after attractant stimulation.

2P-IVM of neutrophil swarms in ear skin

Two-photon intravital imaging of persistent neutrophil swarming in response to a laser-induced focal skin injury has been previously described in detail (*9*). Control and GRK-deficient neutrophils were incubated for 15 min with 1 µM CMFDA and 0.8 µM cell tracker red (CMPTX), or vice-versa, in 1X Hank's balanced salt solution (HBSS) supplemented with 0.0002% (w/v) pluronic F-127. Neutrophils were washed four times with washing buffer (1X HBSS, 1% FBS, 2 mM EDTA), before a 1:1 ratio of differentially dye-labeled control and GRK-deficient neutrophils (each $>2\times10^6$ cells) was taken up in 1X PBS at a volume of 15–30 µl. A 5-µl neutrophil suspension was then injected intradermally with an insulin syringe (31 GA needle, BD Biosciences) into the ventral side of the ear pinnae of an isoflurane-anesthetized $Tyr^{c\text{-}2J/c\text{-}2J}$ recipient mouse. In one experimental set, neutrophils isolated from either $Grk2^{fl/fl}$ $Lifeact\text{-}GFP^{+/-}$ or $Mrp8\text{-}Cre$ $Grk2^{fl/fl}$ $Lifeact\text{-}GFP^{+/-}$ mice were injected into $CAG\text{-}DsRed^{+/+}$ $Tyr^{c\text{-}2J/c\text{-}2J}$ recipient mice to study green-fluorescent injected neutrophils side by side with endogenous red-fluorescent WT neutrophils. Two to three hours after neutrophil injection, mice were again anesthetized using isoflurane (cp-pharma; 2% for induction, 1 to 1.5% for maintenance, vaporized in an 80:20 mixture of oxygen and air) and placed in a lateral recumbent position on a custom-made imaging platform such that the ventral side of the ear pinna rested on a coverslip. A strip of Durapore tape was placed lightly over the ear pinna and affixed to the imaging platform to immobilize the tissue. Anesthetized mice rested in the heated environmental chamber for 30–60 min before a first focal skin injury was induced by a focused two-photon laser pulse at an approximate laser intensity of 80 mW (*9*). At pixel dimensions of 0.14×0.14 µm, a circular region of interest of 25–35 µm in diameter was defined in one focal plane, followed by laser scanning at a pixel dwell time of 0.8 µs for 35–50 iterations, depending on the tissue depth of the imaging field of view. The damage was restricted to dermal layers only. Immediately after laser-induced tissue damage, imaging of the neutrophil response was started at typical voxel dimensions of 0.72×0.72×2 µm. Images were mainly captured towards the anterior half of the ear pinna where hair follicles are sparse. Images were acquired using an inverted LSM 510 NLO (at NIH) or LSM 780 NLO (at MPI Freiburg) multiphoton microscope (Carl Zeiss Microimaging) enclosed in a custom-built environmental chamber that was maintained at 32°C using heated air. These systems were fitted with at least three external non-descanned photomultiplier tube detectors in the reflected light path. Images were acquired using a 25X/0.8 numerical aperture (NA) Plan-Apochromat objective (Carl Zeiss Microimaging) with glycerol as immersion medium. Fluorescence excitation was provided by either a Chameleon XR Ti:Sapphire laser (Coherent) for the LSM 510 NLO or an Insight® Ds+™ (Spectra Physics) for the LSM 780 NLO tuned to 850 nm for dye excitation and the generation of collagen second harmonic signal, or 940 nm for excitation of both DsRed and GFP. Non-descanned detectors collected the emitted light. For four-dimensional data sets, three-dimensional stacks were captured every 30 s, unless otherwise specified. All imaged mice were on the $Tyr^{c\text{-}2J/c\text{-}2J}$ (B6.Albino) background to avoid laser-induced cell death of light-sensitive skin melanophages. Raw imaging data were processed with Imaris (Bitplane) using a Gaussian filter for noise reduction. All movies are displayed as two-dimensional maximum-intensity projections of 10–30 µm thick *z*-stacks.

Mouse infection and 2P-IVM of neutrophil swarms in lymph nodes

GFP-expressing *Pseudomonas aeruginosa PAO1* (PA) (*61*) or *Salmonella typhimurium SL1344* (*62*), both provided through W. Kastenmüller (University Würzburg, Germany), were grown for 1–4 hours in LB medium to reach an OD_{600nm} of 0.6 to 0.7 in the exponential growing culture, before 1×10^7 colony forming units (CFU) of bacteria were diluted in PBS and injected in the mouse foot-pad (20–30 µl), as previously described (*29*). To image endogenous WT and GRK2-depleted neutrophils side-by-side in bacteria-infected lymph nodes, we generated bone marrow chimeric mice. C57BL/6 mice were irradiated with 9 Gray from a ^{137}Cs source and reconstituted with bone marrow from *Ly6g*$^{cre/+}$ *Rosa26*$^{LSL:Tomato}$ mice (WT, TdTomato-expressing neutrophils) and *Mrp8-Cre*$^{+/-}$ *Grk2*$^{fl/fl}$ *Lyz2*$^{gfp/+}$ mice (GRK2-depleted, neutrophils with highest expression of GFP) at a 1:1 ratio. Mice were allowed to reconstitute for at least 8 weeks before imaging analysis. 2P-IVM of transient neutrophil swarms in the subcapsular sinus of bacteria-infected lymph nodes was performed as previously described (*9*). Two to three hours after injection, mice were anesthetized with isoflurane (Baxter; 2% for induction, 1 to 1.5% for maintenance, vaporized in an 80:20 mixture of O_2 and air), before draining popliteal lymph nodes were exposed and intravital microscopy performed. The imaging system was composed of a tuneable Chameleon laser (Coherent) tuned to 930 nm, a wavelength-fixed fiber laser (1055 nm) (Onefive GmbH) and a Zeiss 780 upright microscope equipped with a 20X water immersion lens (NA 1.0, Zeiss) and ZEN acquisition control software. The microscope was enclosed in an environmental chamber in which anesthetized mice were warmed by heated air and the surgically exposed lymph node was kept at 36–37°C with warmed PBS. For 2P-IVM of the subcapsular sinus, a *z*-stack of 40–50 µm, 3-µm step size was used and images were acquired every 40 s. Raw imaging data processing and movie display was similar as for 2P-IVM ear skin data sets. To analyze the containment of bacterial growth in lymph nodes, 1×10^7 colony forming units (CFU) of *P. aeruginosa* PAO1-GFP (PA-GFP) were injected in mouse footpads of *Mrp8-Cre*$^{+/-}$ *Grk2*$^{fl/fl}$ mice and sex- and age-matched littermate control mice. Control mice were either Cre-negative *Grk2*$^{fl/fl}$ or *Mrp8-Cre*$^{+/-}$ *Grk2*$^{+/+}$ mice, depending on the breeder cage set-up. For the quantification of bacterial load, popliteal lymph nodes were harvested 8 hours after infection and lymph node homogenates were plated on blood-agar plates overnight, before bacterial colonies were counted. Neutrophil recruitment into infected popliteal lymph nodes was measured by flow cytometry in single cell suspension of lymph node homogenates 8 hours after infection, identifying neutrophils as a live $Ly6G^+CD11b^+$ leukocyte population. Exclusion criteria for individual values included the absence of bacterial growth or neutrophil recruitment due to improper bacterial injection.

In vitro coculture model

To mimic a bacteria-infected SCS in vitro, macrophages were co-cultured with GFP-expressing *P. aeruginosa* PAO1 (PA-GFP) (*61*) in the presence and absence of neutrophils. Bone marrow-derived mouse macrophages (BMDM) were generated from bone marrow precursors by standard M-CSF culture. Bone marrow cells were suspended in macrophage culture medium and grown over 6 days on Petri dishes in macrophage culture medium (10% FBS, 100 U/ml of penicillin, and 10 µg/ml of streptomycin in RPMI GlutaMax) supplemented with 20 ng/ml of murine M-CSF (PeproTech). PA-GFP were grown in LB medium for 16 hours at 37°C until OD_{600nm} 0.6 to 0.7. When macrophages were infected with bacteria in the absence of neutrophils, experiments were performed in eight-well Lab-Tek imaging chamber slides that were coated with 10 µg/ml fibronectin from human plasma (Sigma-Aldrich, cat no. F2006) overnight at 4°C. For macrophage infection experiments, CellTracker™ Blue-labeled macrophages were taken up in

phenol-red free RPMI supplemented with 10% FCS and 2 mM L-glutamine, then seeded at 80×10^3 cells per well and allowed to adhere for 3 hours at 37°C. PA-GFP in RPMI with 2 mM L-glutamine was then added to BMDM at a ratio of 10 bacteria per one macrophage in the presence of 5 µg/ml propidium iodide (BioLegend). For co-culture experiments of macrophages with bacteria and neutrophils, experiments were performed in µ-Slide VI 0.4 channels (Ibidi, cat no. 80606) that were coated with 10 µg/ml fibronectin overnight at 4°C. Dye-labeled or unlabeled BMDM were seeded at around 15×10^3 cells per channel and allowed to adhere for 3 hours at 37°C. Bacteria and neutrophils were added through separate ports of the slide: 60 µl of the neutrophil suspension at 13×10^6 cells/ml in RPMI with 2 mM L-glutamine and 20% freshly collected mouse serum were added to the first port and 60 µl of PA-GFP (3×10^7 CFU/ml) suspension were added to the second port, before live-cell imaging was initiated. When control and GRK2-depleted neutrophils were analyzed side by side in the well, they were differentially labeled with 5-TAMRA, SE, and CellTracker™ Deep Red, whereas macrophages remained unlabeled. To follow PA-GFP that was phagocytozed by neutrophils, PA-GFP was labeled with 2.5 µg/ml pHrodo™ succinimidyl ester (Thermo Fisher Scientific, cat no. P36600) in 500 µl of freshly prepared 100 mM sodium bicarbonate buffer (pH 8.5) for 30 min at room temperature. Afterwards, bacteria were washed three times with 1X PBS to remove any remaining dye. When visualization of dying cells was required, 5 µg/ml of propidium iodide or 1 µg/ml of DAPI (Sigma-Aldrich) were added to the medium. Macrophage infection with bacteria and neutrophil swarming and clustering were followed by confocal fluorescence laser-scanning microscopy using a confocal LSM 780 microscope (Zeiss) equipped with a stage top incubator to generate an ambient atmosphere of 37°C and 5% CO_2 and objectives. Time-lapse videos were recorded using Plan Apochromat 20X (0.8 NA) and C Apochromat 40X (1.2 NA) objectives with image acquisitions every 5 min over 8 hours, 15 µm *z*-stacks and 2×2 tiled images. Tiled images were stitched during post-processing with ZEN blue software. Images were acquired using up to four-laser line excitation (UV405 for CellTracker™ Blue; Argon488 for PA-GFP, DPSS561 for 5-TAMRA, SE, or SYTOX™ Orange or propidium iodide; HeNe633 for CellTracker™ Deep Red). The internal photomultiplier tubes and GaAsP detector of the confocal system were used for collecting the emitted fluorescence light.

Data analysis of neutrophil in vitro migration

Neutrophil displacement in the under-agarose assay from a starting well toward a chemotactic source well was measured with Imaris software (Bitplane). After 4 hours of chemotaxis, images of neutrophils, which have migrated out of the cell well, were acquired as endpoint measurements and cell center points identified with Imaris spot function. The displacement was measured as the distance between the border of the starting cell well to the migration endpoints of all neutrophils that migrated underneath the agarose toward the attractant well. The mean of all individual displacement values was calculated for each genotype. For displacement ratios, the ratio of WT and $Grk^{-/-}$ neutrophils, which migrated side by side from one well, was calculated and the mean ratios of all four technical replicates determined and plotted as an independent experiment. In some cases (Fig. 1G, and fig. S2A), the mean displacement of all four technical replicates in one dish was determined for WT or $Grk^{-/-}$ and plotted side by side as an independent experiment. In rare cases, technical replicates were excluded from analysis when neutrophils did not respond to the attractant and only very few cells migrated out of the well. Live-cell imaging data of neutrophil chemotaxis in under-agarose assays was visualized (neutrophil trajectories) and analyzed for migration parameters (track length, straightness, *y*-straightness, velocity vector Y, instantaneous speed, and cell roundness) by Imaris manual object cell tracking and statistics

functions. For some experiments, the resultant spatial coordinates over time were further processed to retrieve displacement–time plots by computation using R software (version 4.0.2), R studio (version 1.3.959) and ggplot2 (version 3.3.2). To quantify neutrophil sequential navigation in under-agarose gels with multiple attractant sources (Fig. 3A and fig. S6, B and C), a semi-automated tracking approach was applied. The autoregressive tracking mode of the Imaris spot function was used for automated cell tracking, followed by manual inspection of track validity. Cell displacement lengths in *y*- (toward first gradient/up) and *x*- (toward second gradient/right) directions were derived from Imaris statistic function. To analyze migration arrest in neutrophil clusters (Fig. 4E), individual cells (N=7–22 cells per cluster) were manually tracked over 3–4 hours in cell clusters and instantaneous speed values retrieved from Imaris. Integration into a cluster for longer than 8 min was a criterion for tracking the total movement of a neutrophil. For one cluster, the instantaneous velocities of all cells were determined. An instantaneous speed of <2 µm/min was defined as cell arrest phase, as described previously (*63*). The arrest coefficient was calculated as the percentage of arrest phases from all instantaneous speed values of all cells tracked at one cluster. To analyze the competitive accumulation of neutrophils and eosinophils in clusters during in vitro swarming experiments (Fig. 2, B and I, and fig. S4B), total fluorescent signals of control and *Grk2*$^{-/-}$ cells in the whole cell cluster area were quantified with ImageJ/Fiji software (National Institutes of Health). Accumulation indices were then calculated as the ratio of *Grk2*$^{-/-}$ signal to WT signal on HKSA spots after 2 hours and compared to experiments in which two differentially labeled WT populations formed competitive clusters. Accumulation indices were displayed in graphs with $\log_2$-scaled *y*-axis.

Data analysis of neutrophil in vivo migration

Data from neutrophil migration dynamics recorded with 2P-IVM were visualized (neutrophil trajectories, velocity vector Y, instantaneous speed) and analyzed for migration parameters (track length, straightness, speed) by Imaris manual object cell tracking and statistics functions. To quantify neutrophil clustering in vivo, accumulation indices were calculated. In 2P-IVM laser damage experiments in the skin, the accumulation index as measure of cell entry into the collagen-free zone was defined as the ratio of fluorescent signal from *Grk*$^{-/-}$ cells in the collagen-free zone versus total signal at the wound site divided by the ratio of fluorescent signal from control cells in the collagen-free zone versus total signal at the wound site, as defined previously (*9*). Accumulation indices were calculated when neutrophil cluster size was at its maximum and clusters stabilized. In the skin, this commonly occurred 30–75 min after laser-induced tissue injury, depending on the specific dynamics of an individual neutrophil cluster. Due to the lack of clear collagen signal in lymph node areas, the accumulation index for lymph node infection experiments was defined as the ratio of fluorescent signal from *Grk2*$^{-/-}$ neutrophils in the inner zone (=50% diameter of total cell cluster zone) versus total signal at the whole neutrophil cluster divided by the ratio of fluorescent signal from control cells in the inner zone versus total signal at the neutrophil cluster. Fluorescent signals were quantified with ImageJ/Fiji software. Accumulation indices were displayed in graphs with $\log_2$-scaled *y*-axis. For the display of static images and videos, raw imaging data were processed with Imaris using a Gaussian filter for noise reduction.

Analysis of bacterial growth and phagocytosis in the co-culture assay

Bacterial growth in co-cultures with neutrophils and macrophages was analyzed by quantifying fluorescent signals of GFP-expressing *P. aeruginosa* (PA-GFP) bacteria with Imaris software. By generating surfaces from fluorescent bacteria, "total" bacteria were quantified as total area of PA-

GFP surfaces. To determine the fraction of bacteria "confined" to neutrophil clusters (illustrated in white in Fig. 4B), the surfaces of fluorescent bacteria and CellTracker™-labeled neutrophils were co-localized. Exclusion of co-localization surfaces <250 μm^2 was performed to exclude the very small fraction (4 to 8%) of bacteria-laden individual neutrophils outside of clusters. "Free" bacteria signal outside of neutrophils (illustrated in green in Fig. 4B) was calculated by subtracting the surface areas of "confined" bacteria to neutrophils from "total" bacteria. To quantify the fraction of pHrodo™-tagged, phagocytosed PA-GFP, the fluorescence of the pHrodo™ signal was measured per neutrophil cell cluster using Imaris software. To quantify bacteria containment within neutrophil clusters, we used ImageJ/Fiji software to draw two outlines around a bacteria cluster surrounded neutrophils: one defined the perimeter of the complete bacteria cluster, the other defined the perimeter part in direct contact with clustering neutrophils. Bacteria containment was calculated as the percentage of the perimeter in direct contact with neutrophils from the complete bacteria cluster perimeter.

Determination of knockout efficiencies

To determine knockout efficiencies in neutrophils isolated from conditional knockout mice, quantitative real-time PCR (qRT-PCR) and immunoblot analysis were performed. For qRT-PCR, total RNA of bone marrow neutrophils was extracted using TRI Reagent™ solution (Sigma-Aldrich). Briefly, the aqueous RNA containing phase was extracted with chloroform. The RNA was precipitated in 2-propanol overnight at −20°C. The RNA pellet was washed twice in 80% ethanol. DNase treatment was performed using TURBO DNA-free™ Kit (Ambion). Reverse transcription was performed using SuperScript™ II reverse transcriptase and random hexamer primers following the manufacturer's instructions (Invitrogen). Quantitative PCR was performed using a SYBR™ Green master mix cocktail (Thermo Fisher Scientific). cDNA amplification and quantification were performed in a StepOnePlus real-time PCR machine (Applied Biosystems). Gene expression levels of *Grk2*, *Grk3*, *Grk5* and *Grk6* were normalized against *18S rRNA*, *B2m* and *Actb* as reference genes. See table S2 for details on primers. For immunoblot analysis, neutrophils were first lysed in freshly prepared RIPA buffer (50 mM Tris-HCl, 150 mM NaCl, 1.0% (v:v) IGEPAL® CA-630, 1% (v:v) Triton™ X- 100, 5 mM EGTA, 5 mM EDTA, and 1X cOmplete™ protease inhibitor cocktail). Proteins were separated by 4–12% SDS-PAGE gels (BioRad) and then transferred onto PVDF membranes (Millipore) and nonspecific binding was blocked with 5% BSA (Sigma-Aldrich) in tris-buffered saline containing 0.1% Tween-20, followed by overnight incubation with primary antibodies against GRK2 (SCBT) and actin as control (Sigma-Aldrich). Membranes were subsequently washed and incubated with the appropriate secondary antibodies (Dako), and immunoreactivity was detected upon incubation with Clarity Western ECL substrate (BioRad) using ChemiDoc Imaging System (BioRad). The same protocol was used for the determination of GRK2 knockout efficiency in eosinophils (see below). For details on the use of antibodies, we refer to table S4.

Flow cytometric analysis of neutrophil subpopulations

Neutrophil subsets in bone marrow and blood were analyzed by flow cytometry as previously described (*64*). Unspecific binding was blocked with anti-mouse CD16/CD32. Fixable Viability Dye eFluor506 (Thermo Fisher Scientific) was used to stain dead cells. Antibodies and reagents used for flow cytometry are summarized in table S4. Flow cytometric analysis was performed using an LSRFortessa™ (BD Biosciences) flow cytometer, FACSDiva™ software (BD Biosciences) and FlowJo software (FlowJo, LLC). For the analysis of neutrophils in the bone

marrow, gating started with Lineage (B220, CD3e, CD90.2, NK1.1)$^-$ cells. Blood neutrophils were gated on (Lineage$^-$, CD115$^-$, SiglecF$^-$, Gr1$^+$, CD11b$^+$) cells.

Receptor internalization

Surface receptor expression after ligand stimulation was measured by flow cytometry. Neutrophils were stimulated with 200 nM LTB4 or 50 nM CXCL2 for the indicated time points at 37°C. Then, cells were incubated on ice to halt receptor internalization. Flow cytometric staining for LTB4R1 and CXCR2 (see table S4 for details on antibodies) was performed as described with all steps at 4°C.

Neutrophil GPCR desensitization: MAPK signaling and GPCR-induced chemokinesis

To measure activation of MAPK signaling cascades downstream of GPCR activation, neutrophils were stimulated with GPCR ligands (LTB4, CXCL2, C5a) for the indicated time points followed by fixation in 1.6% paraformaldehyde (Thermo Fisher Scientific) and permeabilization in 100% methanol at −20°C overnight. Cells were stimulated with individual attractants for 2 min. For triple stimulations with increasing concentrations of LTB4 (50 nM, 100 nM, and 200 nM), CXCL2 (50 nM, 100 nM, and 200 nM), or C5a (5 nM, 10 nM, and 20 nM), cells were treated for 4 min (first stimulation), 4 min (second stimulation), and 2 min (third stimulation). For the intracellular antibody stainings, nonspecific binding was blocked with anti-mouse CD16/CD32 and 5% rabbit serum (Thermo Fisher Scientific) in 1X PBS. Neutrophils were then stained with directly fluorescent anti-mouse antibodies against p-p38 MAPK and p-p44/42 (see table S4). Flow cytometric analysis was performed using an LSRFortessa™ (BD Biosciences) flow cytometer, FACSDiva™ software (BD Biosciences) and FlowJo software (FlowJo, LLC).

To measure the effect of GPCR desensitization on chemokinesis, WT and *Grk2*$^{-/-}$ neutrophils were pre-treated with attractant concentrations that desensitize GPCR-induced calcium responses in WT cells: LTB4 (50 nM, 100 nM, and 200 nM), CXCL2 (50 nM, 100 nM), and CXCL2 (10 nM, 20 nM, 40 nM) according to the time scheme described before. For these experiments, WT and *Grk2*$^{-/-}$ neutrophils were isolated from *Mrp8-Cre Grk2*$^{+/+}$ *R26*$^{LSL:Tom}$ (WT, red) and *Mrp8-Cre Grk2*$^{fl/fl}$ *Lyz2*$^{Gfp/+}$ (*Grk2*$^{-/-}$, green) mice, or alternatively from *Mrp8-Cre Grk2*$^{fl/fl}$ *R26*$^{LSL:Tom}$ (KO, red) and *Mrp8-Cre Grk2*$^{+/+}$ *Lyz2*$^{Gfp/+}$ (WT, green) mice. Pre-treated, differentially color-labeled WT and *Grk2*$^{-/-}$ neutrophils were loaded into the same µ-Slide VI 0.4 channel, which was coated with human recombinant ICAM-1 (Peprotech, 1 µg/ml), and were immediately imaged side by side with confocal spinning-disk microscopy. We have used the Cell Observer SD system (Zeiss) comprising a CSU-X1 confocal scanner unit (Yokogawa) mounted on an AxioObserver Z1 inverted microscope stand, and equipped with a Prime BSI back-illuminated CMOS camera (Teledyne Photometrics). A Plan-Apochromat 10X 0.45 objective (Zeiss) and excitation with 488 nm and 561 nm solid state lasers were used in order to observe neutrophils with a frame rate of 30 seconds over 45 minutes. Randomly chosen cells were tracked with Imaris spot function and statistics function to retrieve cell positions for the display of cell tracks with R ggplot2 function.

Assays for neutrophil effector functions

Neutrophil myeloperoxidase (MPO) release was measured with ELISA according to the manufacturer's instructions (R&D Systems; cat no. DY3667). Neutrophil elastase (NE) activity was determined using the EnzCheck™ elastase assay kit following the manufacturer's instructions (Thermo Fisher Scientific; cat no. E12056). MPO and NE release were determined in supernatants of neutrophils stimulated with 100 nM LTB4 and 100 nM CXCL2 for 2 hours.

Reactive oxygen species (ROS) production was quantified by determining the superoxide dismutase (SOD) inhibitable reduction of (ferri-) cytochrome c as previously described (*65*). Briefly, neutrophils were stimulated with 100 nM LTB4 and 100 nM CXCL2, heat-killed *P. aeruginosa* bioparticles (HKPA, at a ratio of 100 particles to one cell) (Invivogen), 10 µg/ml zymosan (Thermo Fisher Scientific) or 10 nM phorbol-12-myristat-13-acetat (PMA, Sigma-Aldrich) in the presence of 100 µM cytochrome c from equine heart (Thermo Fisher Scientific). As control for non-specific cytochrome c reduction, simultaneous assays were performed in the presence of 100 U/ml of SOD, and the SOD-inhibitable signal was determined. The release of ROS was measured every minute for 1 hour by light absorbance at 550 nm (wavelength correction at 490 nm) using a Synergy4 plate reader (Bio-Tek) heated to 37°C. As standard measure for neutrophil phagocytosis, neutrophils were co-incubated for 1 hour with opsonized *S. aureus* pHrodo™ bioparticles (Thermo Fisher Scientific; cat no. A10010) at a ratio of 100:1 in the absence or presence of LTB4 and CXCL2 (100 nM each), before particle uptake was analyzed by flow cytometry. To measure internalization of living *P. aeruginosa*, TdTomato-expressing neutrophils were co-incubated with PAO1-GFP at MOI=20. Cells and bacteria were co-incubated in a 1.5 ml reaction tube in a total volume of 100 µl of phenol-red free RPMI supplemented with 20% mouse serum (VWR, cat no. S2160-050) and 2 mM L-glutamine in the absence or presence of LTB4/CXCL2 (100 nM each), and placed in a shaking heat block at 450 rpm, 37°C for 60 min. TdTomato-expressing WT or *Grk2*$^{-/-}$ neutrophils were isolated from *Mrp8-Cre Grk2*$^{+/+}$ *R26*$^{LSL:Tom}$ or *Mrp8-Cre Grk2*$^{fl/fl}$ *R26*$^{LSL:Tom}$ mice, respectively. After the one-hour co-incubation 60 µl of the cell–bacteria suspension was transferred into µ-Slide VI 0.4 channels (Ibidi). Fluorescent neutrophils and bacteria were imaged with a confocal LSM 780 microscope (Zeiss) equipped with a stage-top incubator to generate an ambient atmosphere of 37°C and 5% CO_2. Images were recorded using Plan Apochromat 20X (0.8 NA) at 1024×1024 resolution and 7×7 tiles. Imaris surface and spot functions were used to determine GFP-positive signals located inside surfaces of red neutrophils (as shown in fig. S8B). Per experimental condition, approximately 200-1000 neutrophils were analyzed and the percentage of neutrophils with internalized bacteria was calculated. To identify and quantify NET-like structures in the co-culture assay with PAO1-GFP and macrophages, 10 nM SYTOX™ Orange nucleic acid stain (Thermo Fisher Scientific) was added to the medium. Confocal microscopy of SYTOX™ Orange fluorescent signal was recorded, before surfaces of the SYTOX™ Orange fluorescent signal were generated with Imaris software. Total surface areas were quantified after exclusion of surfaces <250 µm^2 that were considered non-NET-like structures.

Design and statistical analysis

Sample size was determined prior to experiment for all experiments used for hypothesis testing (i.e. data that include statistical inference). Sample size for animal experimentation was determined according to animal welfare guidelines. Reproducibility of the experimental findings was verified using biological replicates. Experimental groups were defined by the genotype. Blinding was not relevant to our study because all experimental groups (genotyping groups) were treated the same. Unpaired two-tailed *t* tests, paired *t* tests for ratios and analysis of variance (ANOVA) were performed after data were confirmed to fulfill the criteria of normal distribution and equal variance, otherwise two-tailed Kruskal–Wallis tests or Mann–Whitney *U* tests were applied. If overall ANOVA or Kruskal–Wallis tests were significant, we performed post hoc test with pair-wise comparisons (ANOVA: Tukey, Kruskal–Wallis: Dunn). Analyses were performed with GraphPad Prism-software (8.2.1 and 9.0.2). For further statistical details, see table S3.

References:

1. M. D. Breed, E. Guzman-Novoa, G. J. Hunt, Defensive behavior of honey bees: organization, genetics, and comparisons with other bees. *Annu. Rev. Entomol.* **49**, 271-298 (2004).
2. X. Guo *et al.*, 4-Vinylanisole is an aggregation pheromone in locusts. *Nature* **584**, 584-588 (2020).
3. D. C. Mahadeo, C. A. Parent, Signal relay during the life cycle of Dictyostelium. *Curr. Top. Dev. Biol.* **73**, 115-140 (2006).
4. K. Ley *et al.*, Neutrophils: New insights and open questions. *Sci. Immunol.* **3**, (2018).
5. A. S. W. Neupane *et al.*, Patrolling Alveolar Macrophages Conceal Bacteria from the Immune System to Maintain Homeostasis. *Cell* **183**, 110-125 (2020).
6. S. Uderhardt, A. J. Martins, J. S. Tsang, T. Lämmermann, R. N. Germain, Resident Macrophages Cloak Tissue Microlesions to Prevent Neutrophil-Driven Inflammatory Damage. *Cell* **177**, 541-555 (2019).
7. K. Kienle, T. Lämmermann, Neutrophil swarming: an essential process of the neutrophil tissue response. *Immunol. Rev.* **273**, 76-93 (2016).
8. W. Weninger, M. Biro, R. Jain, Leukocyte migration in the interstitial space of non-lymphoid organs. *Nat. Rev. Immunol.* **14**, 232-246 (2014).
9. T. Lämmermann *et al.*, Neutrophil swarms require LTB4 and integrins at sites of cell death in vivo. *Nature* **498**, 371-375 (2013).
10. C. Coombs *et al.*, Chemokine receptor trafficking coordinates neutrophil clustering and dispersal at wounds in zebrafish. *Nat. Commun.* **10**, 5166 (2019).
11. H. Poplimont *et al.*, Neutrophil Swarming in Damaged Tissue Is Orchestrated by Connexins and Cooperative Calcium Alarm Signals. *Curr. Biol.* **30**, 2761-2776 (2020).
12. E. Reategui *et al.*, Microscale arrays for the profiling of start and stop signals coordinating human-neutrophil swarming. *Nat. Biomed. Eng.* **1**, 0094 (2017).
13. N. J. Freedman, R. J. Lefkowitz, Desensitization of G protein-coupled receptors. *Recent Prog. Horm. Res.* **51**, 319-351; discussion 352-313 (1996).
14. T. Lämmermann, W. Kastenmüller, Concepts of GPCR-controlled navigation in the immune system. *Immunol. Rev.* **289**, 205-231 (2019).

15. J. J. Rose, J. F. Foley, P. M. Murphy, S. Venkatesan, On the mechanism and significance of ligand-induced internalization of human neutrophil chemokine receptors CXCR1 and CXCR2. *J. Biol. Chem.* **279**, 24372-24386 (2004).
16. E. D. Tomhave *et al.*, Cross-desensitization of receptors for peptide chemoattractants. Characterization of a new form of leukocyte regulation. *J. Immunol.* **153**, 3267-3275 (1994).
17. J. Fan, A. B. Malik, Toll-like receptor-4 (TLR4) signaling augments chemokine-induced neutrophil migration by modulating cell surface expression of chemokine receptors. *Nat. Med.* **9**, 315-321 (2003).
18. A. Kavelaars *et al.*, Increased acute inflammation, leukotriene B4-induced chemotaxis, and signaling in mice deficient for G protein-coupled receptor kinase 6. *J. Immunol.* **171**, 6128-6134 (2003).
19. S. K. Raghuwanshi *et al.*, The chemokine receptors CXCR1 and CXCR2 couple to distinct G protein-coupled receptor kinases to mediate and regulate leukocyte functions. *J. Immunol.* **189**, 2824-2832 (2012).
20. T. K. Tarrant *et al.*, G protein-coupled receptor kinase-3-deficient mice exhibit WHIM syndrome features and attenuated inflammatory responses. *J. Leukoc. Biol.* **94**, 1243-1251 (2013).
21. A. Vroon *et al.*, GRK6 deficiency is associated with enhanced CXCR4-mediated neutrophil chemotaxis in vitro and impaired responsiveness to G-CSF in vivo. *J. Leukoc. Biol.* **75**, 698-704 (2004).
22. T. I. Arnon *et al.*, GRK2-dependent S1PR1 desensitization is required for lymphocytes to overcome their attraction to blood. *Science* **333**, 1898-1903 (2011).
23. T. Evron, T. L. Daigle, M. G. Caron, GRK2: multiple roles beyond G protein-coupled receptor desensitization. *Trends Pharmacol. Sci.* **33**, 154-164 (2012).
24. Y. Aratake *et al.*, Helix 8 of leukotriene B4 receptor 1 inhibits ligand-induced internalization. *FASEB J.* **26**, 4068-4078 (2012).
25. B. C. Subramanian, K. Moissoglu, C. A. Parent, The LTB4-BLT1 axis regulates the polarized trafficking of chemoattractant GPCRs during neutrophil chemotaxis. *J. Cell Sci.* **131**, (2018).

26. H. K. Mishra, C. Long, N. S. Bahaie, B. Walcheck, Regulation of CXCR2 expression and function by a disintegrin and metalloprotease-17 (ADAM17). *J. Leukoc. Biol.* **97**, 447-454 (2015).

27. M. L. Patnode, J. K. Bando, M. F. Krummel, R. M. Locksley, S. D. Rosen, Leukotriene B4 amplifies eosinophil accumulation in response to nematodes. *J. Exp. Med.* **211**, 1281-1288 (2014).

28. E. F. Foxman, J. J. Campbell, E. C. Butcher, Multistep navigation and the combinatorial control of leukocyte chemotaxis. *J. Cell. Biol.* **139**, 1349-1360 (1997).

29. W. Kastenmüller, P. Torabi-Parizi, N. Subramanian, T. Lämmermann, R. N. Germain, A spatially-organized multicellular innate immune response in lymph nodes limits systemic pathogen spread. *Cell* **150**, 1235-1248 (2012).

30. D. Dacheux, J. Goure, J. Chabert, Y. Usson, I. Attree, Pore-forming activity of type III system-secreted proteins leads to oncosis of Pseudomonas aeruginosa-infected macrophages. *Mol. Microbiol.* **40**, 76-85 (2001).

31. A. Thanabalasuriar *et al.*, Neutrophil Extracellular Traps Confine Pseudomonas aeruginosa Ocular Biofilms and Restrict Brain Invasion. *Cell Host Microbe* **25**, 526-536 (2019).

32. B. Heit, S. Tavener, E. Raharjo, P. Kubes, An intracellular signaling hierarchy determines direction of migration in opposing chemotactic gradients. *J. Cell. Biol.* **159**, 91-102 (2002).

33. A. Hopke *et al.*, Neutrophil swarming delays the growth of clusters of pathogenic fungi. *Nat. Commun.* **11**, 2031 (2020).

34. J. C. Waite *et al.*, Dynamic imaging of the effector immune response to listeria infection in vivo. *PLoS Pathog.* **7**, e1001326 (2011).

35. X. Liu *et al.*, Bidirectional regulation of neutrophil migration by mitogen-activated protein kinases. *Nat. Immunol.* **13**, 457-464 (2012).

36. G. Wang *et al.*, Oxidant Sensing by TRPM2 Inhibits Neutrophil Migration and Mitigates Inflammation. *Dev. Cell* **38**, 453-462 (2016).

37. M. Chabaud *et al.*, Cell migration and antigen capture are antagonistic processes coupled by myosin II in dendritic cells. *Nat. Commun.* **6**, 7526 (2015).

38. I. R. Evans, P. A. Ghai, V. Urbancic, K. L. Tan, W. Wood, SCAR/WAVE-mediated processing of engulfed apoptotic corpses is essential for effective macrophage migration in Drosophila. *Cell Death Differ.* **20**, 709-720 (2013).
39. G. Faure-Andre *et al.*, Regulation of dendritic cell migration by CD74, the MHC class II-associated invariant chain. *Science* **322**, 1705-1710 (2008).
40. I. Lavi, M. Piel, A. M. Lennon-Dumenil, R. Voituriez, N. S. Gov, Deterministic patterns in cell motility. *Nat. Physics* **12**, 1146-1152 (2016).
41. M. Pan, X. Xu, Y. Chen, T. Jin, Identification of a Chemoattractant G-Protein-Coupled Receptor for Folic Acid that Controls Both Chemotaxis and Phagocytosis. *Dev. Cell* **36**, 428-439 (2016).
42. D. M. Veltman, M. G. Lemieux, D. A. Knecht, R. H. Insall, PIP(3)-dependent macropinocytosis is incompatible with chemotaxis. *J. Cell. Biol.* **204**, 497-505 (2014).
43. X. Wen *et al.*, G-protein-coupled formyl peptide receptors play a dual role in neutrophil chemotaxis and bacterial phagocytosis. *Mol. Biol. Cell* **30**, 346-356 (2019).
44. Y. H. Dong, L. H. Zhang, Quorum sensing and quorum-quenching enzymes. *J. Microbiol.* **43 Spec No**, 101-109 (2005).
45. L. Tweedy *et al.*, Seeing around corners: Cells solve mazes and respond at a distance using attractant breakdown. *Science* **369**, eaay9792 (2020).
46. E. Passegue, E. F. Wagner, I. L. Weissman, JunB deficiency leads to a myeloproliferative disorder arising from hematopoietic stem cells. *Cell* **119**, 431-443 (2004).
47. S. J. Matkovich *et al.*, Cardiac-specific ablation of G-protein receptor kinase 2 redefines its roles in heart development and beta-adrenergic signaling. *Circ. Res.* **99**, 996-1003 (2006).
48. K. Peppel *et al.*, G protein-coupled receptor kinase 3 (GRK3) gene disruption leads to loss of odorant receptor desensitization. *J. Biol. Chem.* **272**, 25425-25428 (1997).
49. R. R. Gainetdinov *et al.*, Muscarinic supersensitivity and impaired receptor desensitization in G protein-coupled receptor kinase 5-deficient mice. *Neuron* **24**, 1029-1036 (1999).
50. R. R. Gainetdinov *et al.*, Dopaminergic supersensitivity in G protein-coupled receptor kinase 6-deficient mice. *Neuron* **38**, 291-303 (2003).

51. N. Faust, F. Varas, L. M. Kelly, S. Heck, T. Graf, Insertion of enhanced green fluorescent protein into the lysozyme gene creates mice with green fluorescent granulocytes and macrophages. *Blood* **96**, 719-726 (2000).

52. A. Hasenberg *et al.*, Catchup: a mouse model for imaging-based tracking and modulation of neutrophil granulocytes. *Nat. Methods* **12**, 445-452 (2015).

53. J. de Boer *et al.*, Transgenic mice with hematopoietic and lymphoid specific expression of Cre. *Eur. J. Immunol.* **33**, 314-325 (2003).

54. K. Vintersten *et al.*, Mouse in red: red fluorescent protein expression in mouse ES cells, embryos, and adult animals. *Genesis* **40**, 241-246 (2004).

55. E. D. Hughes *et al.*, Genetic variation in C57BL/6 ES cell lines and genetic instability in the Bruce4 C57BL/6 ES cell line. *Mamm. Genome* **18**, 549-558 (2007).

56. D. Townsend, C. J. Witkop, Jr., J. Mattson, Tyrosinase subcellular distribution and kinetic parameters in wild type and C-locus mutant C57BL/6J mice. *J. Exp. Zool.* **216**, 113-119 (1981).

57. J. Riedl *et al.*, Lifeact mice for studying F-actin dynamics. *Nat. Methods* **7**, 168-169 (2010).

58. B. Heit, P. Kubes, Measuring chemotaxis and chemokinesis: the under-agarose cell migration assay. *Sci STKE* **2003**, PL5 (2003).

59. S. Wang, J. P. Dangerfield, R. E. Young, S. Nourshargh, PECAM-1, alpha6 integrins and neutrophil elastase cooperate in mediating neutrophil transmigration. *J. Cell Sci.* **118**, 2067-2076 (2005).

60. K. D. Dyer *et al.*, Functionally competent eosinophils differentiated ex vivo in high purity from normal mouse bone marrow. *J. Immunol.* **181**, 4004-4009 (2008).

61. D. G. Davies *et al.*, The involvement of cell-to-cell signals in the development of a bacterial biofilm. *Science* **280**, 295-298 (1998).

62. S. K. Hoiseth, B. A. Stocker, Aromatic-dependent Salmonella typhimurium are non-virulent and effective as live vaccines. *Nature* **291**, 238-239 (1981).

63. G. Shakhar *et al.*, Stable T cell-dendritic cell interactions precede the development of both tolerance and immunity in vivo. *Nat. Immunol.* **6**, 707-714 (2005).

64. M. Evrard et al., Developmental Analysis of Bone Marrow Neutrophils Reveals Populations Specialized in Expansion, Trafficking, and Effector Functions. *Immunity* 48, 364-379 e368 (2018).

65. B. K. Rada, M. Geiszt, K. Kaldi, C. Timar, E. Ligeti, Dual role of phagocytic NADPH oxidase in bacterial killing. *Blood* 104, 2947-2953 (2004).

Acknowledgments: We thank R. Wedlich-Söldner for kindly providing mice for this study; R. Thünauer and W. Römer for initial help with bacterial work; D. Legler for helpful advice; members of the MPI Imaging Facility for assistance with imaging; and K. Ganter and L. Kaltenbach for assistance with experiments and analysis. **Funding:** Supported by the Max Planck Society (T.L., W.K.); the Deutsche Forschungsgemeinschaft (LA3465/1-1, SFB/CRC167, and CRC850-A03, T.L.; Germany's Excellence Strategy EXC-294 and EXC-2189:390939984, CRC850-A06, and CRC1381-B09, R.B.); European Union Horizon 2020 ERC Starting Grant 715890 (T.L.); European Union Horizon 2020 ERC Consolidator Grant 819329 (W.K.); the Ministry of Culture and Science of North Rhine-Westphalia, the Governing Mayor of Berlin including Science and Research, and the Federal Ministry of Education and Research (BMBF) (M.G.); the Chan Zuckerberg Initiative Grant 2020-217723 (E.R., T.L.); the Intramural Research Program of the National Institute of Allergy and Infectious Diseases, National Institutes of Health (R.N.G.) and NIAID grant AI13937 (D.I.). **Author contributions:** K.Ki. and K.M.G.: conceptualization, investigation, methodology, validation, formal analysis, visualization, and writing review and editing; K.M.G.: software; S.E. and K.Kn.: investigation and methodology; M.M. and M.W.E.: investigation; M.G., R.B., T.T.: resources; R.N.G.: writing review and editing; E.R. and D.I.: resources, methodology; W.K.: methodology and writing review and editing; T.L.: conceptualization, funding acquisition, project administration, supervision, investigation, formal analysis, methodology, visualization, writing original draft; ICMJE guidelines were taken into consideration. **Competing interests:** The authors declare no competing interests. **Data and materials availability:** All data are available in the main text or the supplementary materials. The use of *Grk3*-deficient mice was restricted by a material transfer agreement with Duke University. The source code for generating displacement–time plots is available at: https://github.com/KMGlaser/Kienle-et-al.git. Materials and raw data are available from the corresponding author, T.L..

Supplementary Materials:

Figures S1-S10
Tables S1-S4

Fig. 1

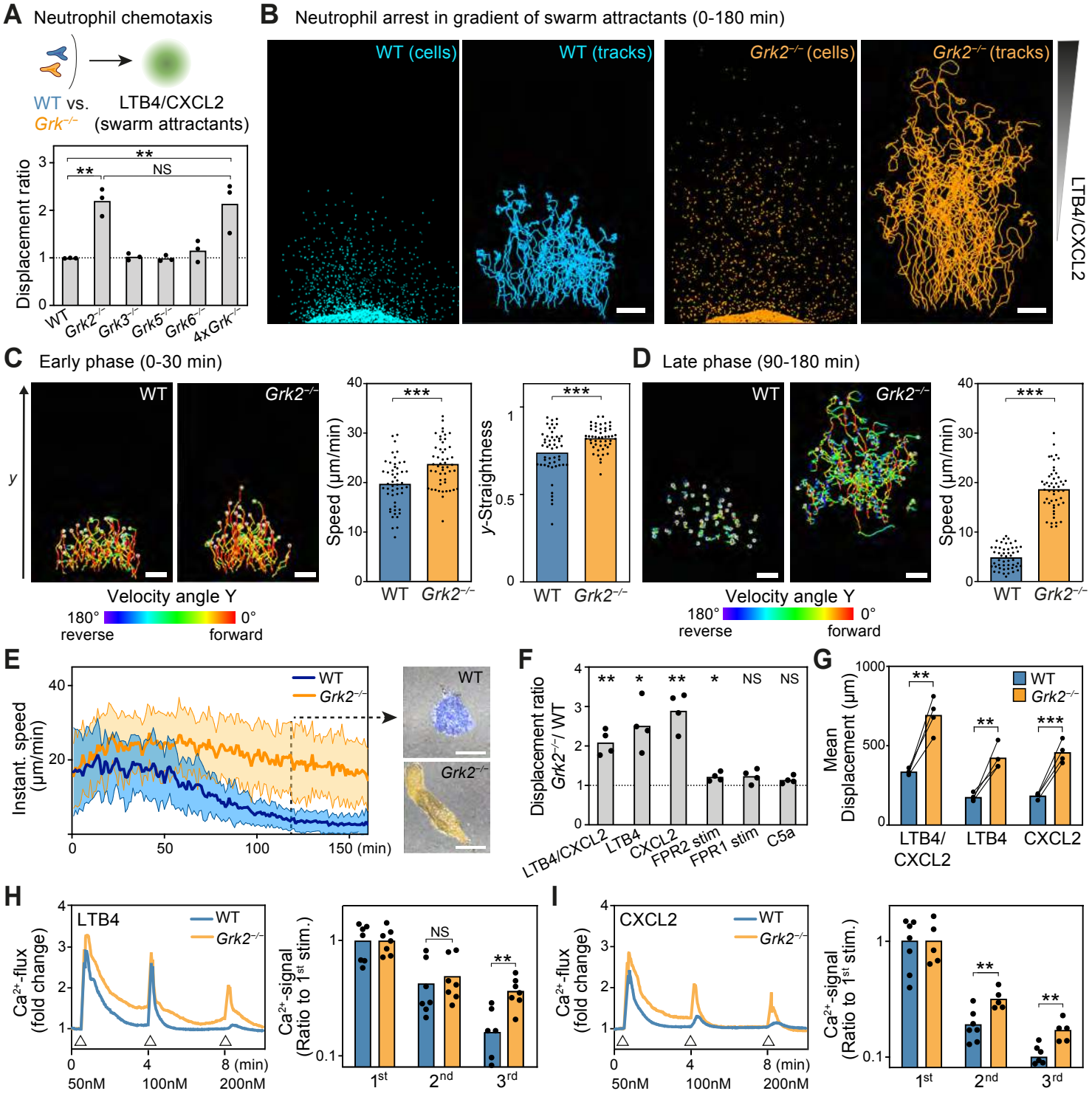
A Neutrophil chemotaxis
WT vs. Grk−/−
LTB4/CXCL2 (swarm attractants)
Displacement ratio
WT
Grk2−/−
Grk3−/−
Grk5−/−
Grk6−/−
4xGrk−/−
B Neutrophil arrest in gradient of swarm attractants (0-180 min)
WT (cells)
WT (tracks)
Grk2−/− (cells)
Grk2−/− (tracks)
LTB4/CXCL2
C Early phase (0-30 min)
WT
Grk2−/−
y
Velocity angle Y
180° reverse
0° forward
Speed (µm/min)
y-Straightness
D Late phase (90-180 min)
E
Instant. speed (µm/min)
150 (min)
F
Displacement ratio Grk2−/− / WT
LTB4/CXCL2
LTB4
CXCL2
FPR2 stim
FPR1 stim
C5a
G
Mean Displacement (µm)
LTB4/ CXCL2
H
LTB4
Ca2+-flux (fold change)
Ca2+-signal (Ratio to 1st stim.)
50nM
100nM
200nM
I
CXCL2

Fig. 2

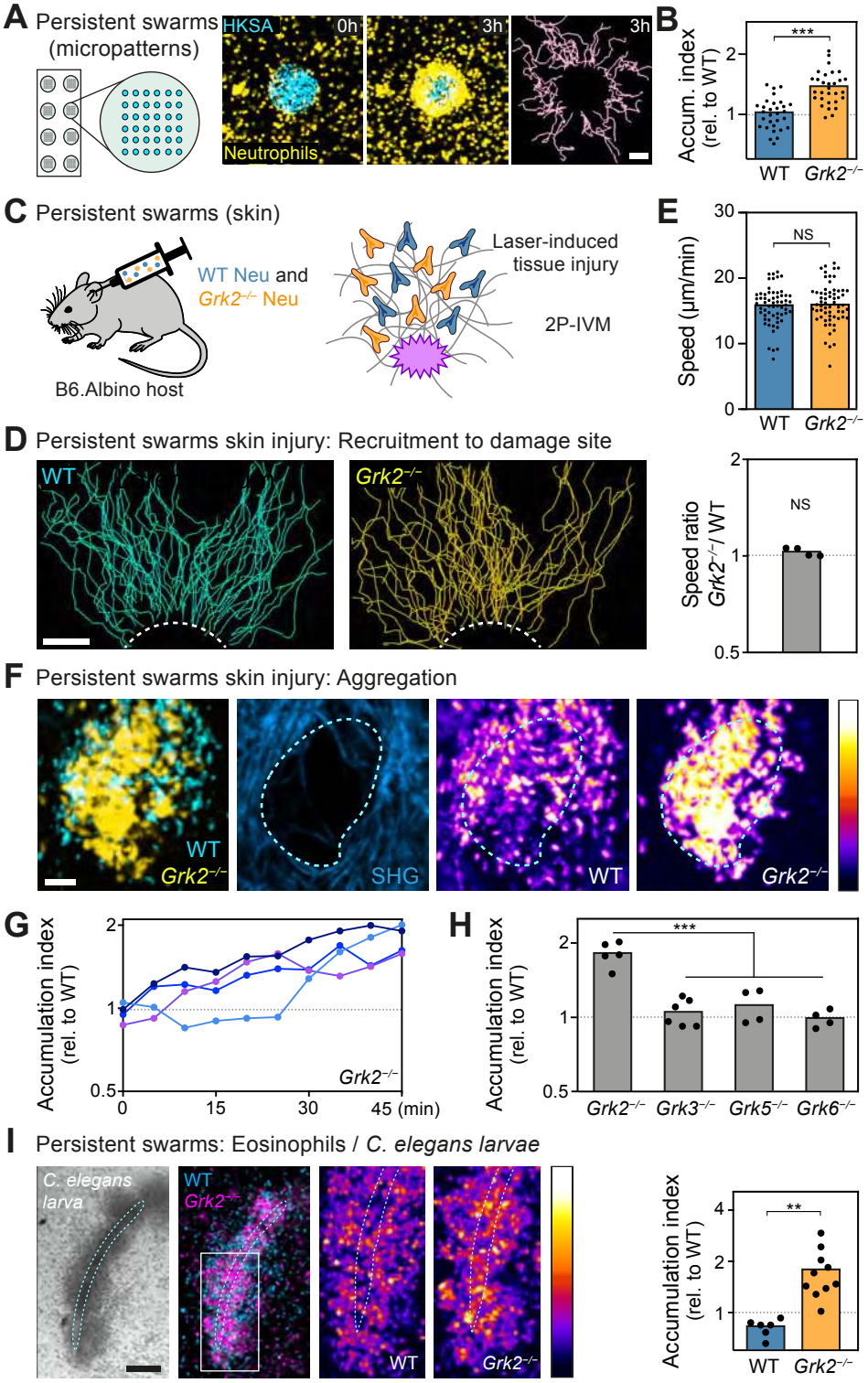
A Persistent swarms (micropatterns)
HKSA
0h
3h
3h
Neutrophils
B
Accum. index (rel. to WT)
***
WT
Grk2−/−
C Persistent swarms (skin)
WT Neu and Grk2−/− Neu
B6.Albino host
Laser-induced tissue injury
2P-IVM
E
Speed (μm/min)
NS
WT
Grk2−/−
D Persistent swarms skin injury: Recruitment to damage site
WT
Grk2−/−
Speed ratio Grk2−/− / WT
NS
F Persistent swarms skin injury: Aggregation
WT
Grk2−/−
SHG
WT
Grk2−/−
G
Accumulation index (rel. to WT)
Grk2−/−
0
15
30
45 (min)
H
Accumulation index (rel. to WT)
***
Grk2−/−
Grk3−/−
Grk5−/−
Grk6−/−
I Persistent swarms: Eosinophils / C. elegans larvae
C. elegans larva
WT
Grk2−/−
WT
Grk2−/−
Accumulation index (rel. to WT)
**
WT
Grk2−/−

Fig.3

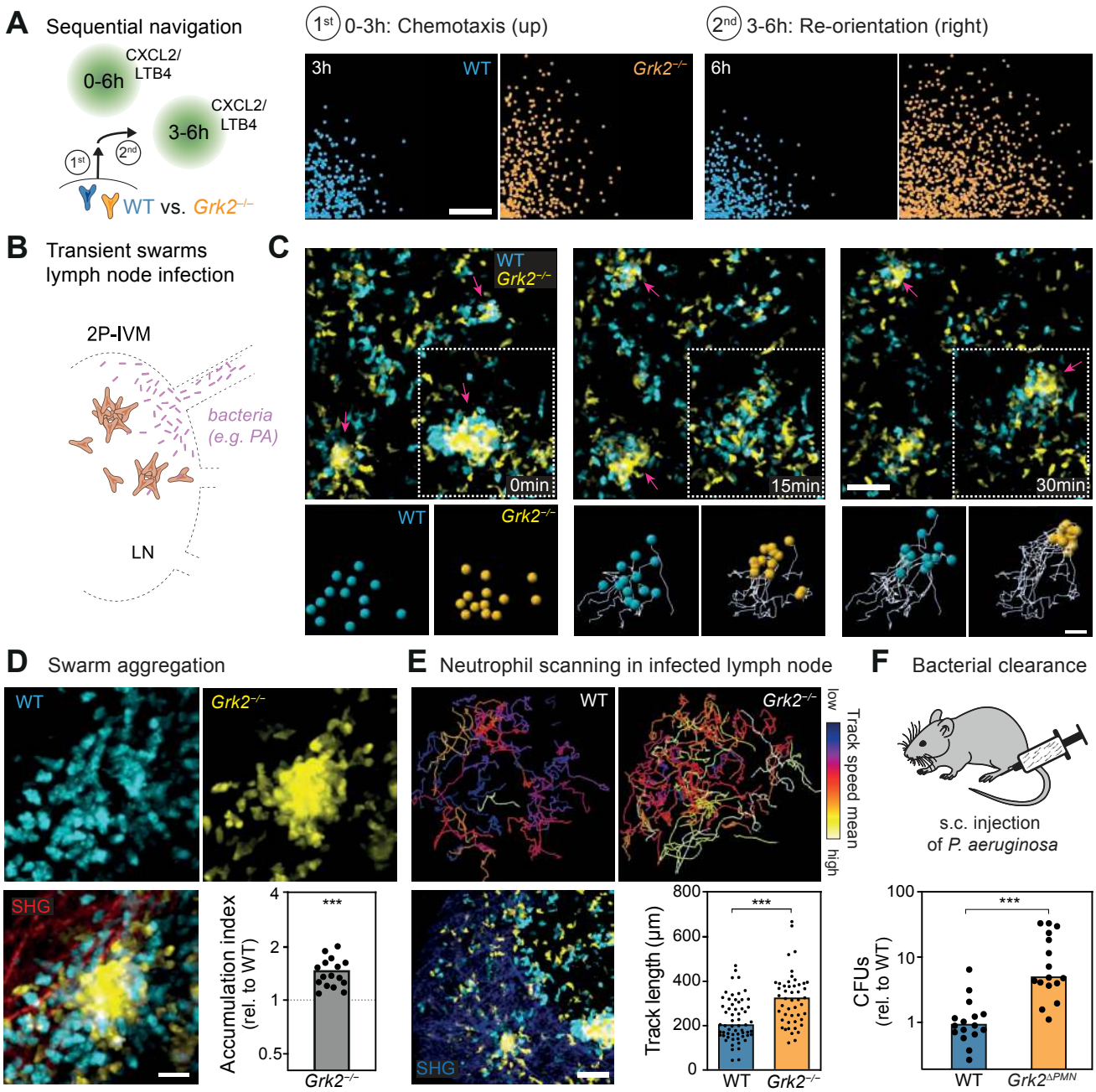
A
Sequential navigation
CXCL2/
LTB4
0-6h
CXCL2/
LTB4
3-6h
1st
2nd
WT vs. Grk2−/−
1st 0-3h: Chemotaxis (up)
2nd 3-6h: Re-orientation (right)
3h
WT
Grk2−/−
6h
B
Transient swarms
lymph node infection
2P-IVM
bacteria
(e.g. PA)
LN
C
WT
Grk2−/−
0min
15min
30min
WT
Grk2−/−
D
Swarm aggregation
WT
Grk2−/−
SHG
Accumulation index
(rel. to WT)
4
2
1
0.5
***
Grk2−/−
E
Neutrophil scanning in infected lymph node
WT
Grk2−/−
low
high
Track speed mean
SHG
Track length (µm)
800
600
400
200
0
***
WT
Grk2−/−
F
Bacterial clearance
s.c. injection
of P. aeruginosa
CFUs
(rel. to WT)
100
10
1
***
WT
Grk2ΔPMN

Fig. 4

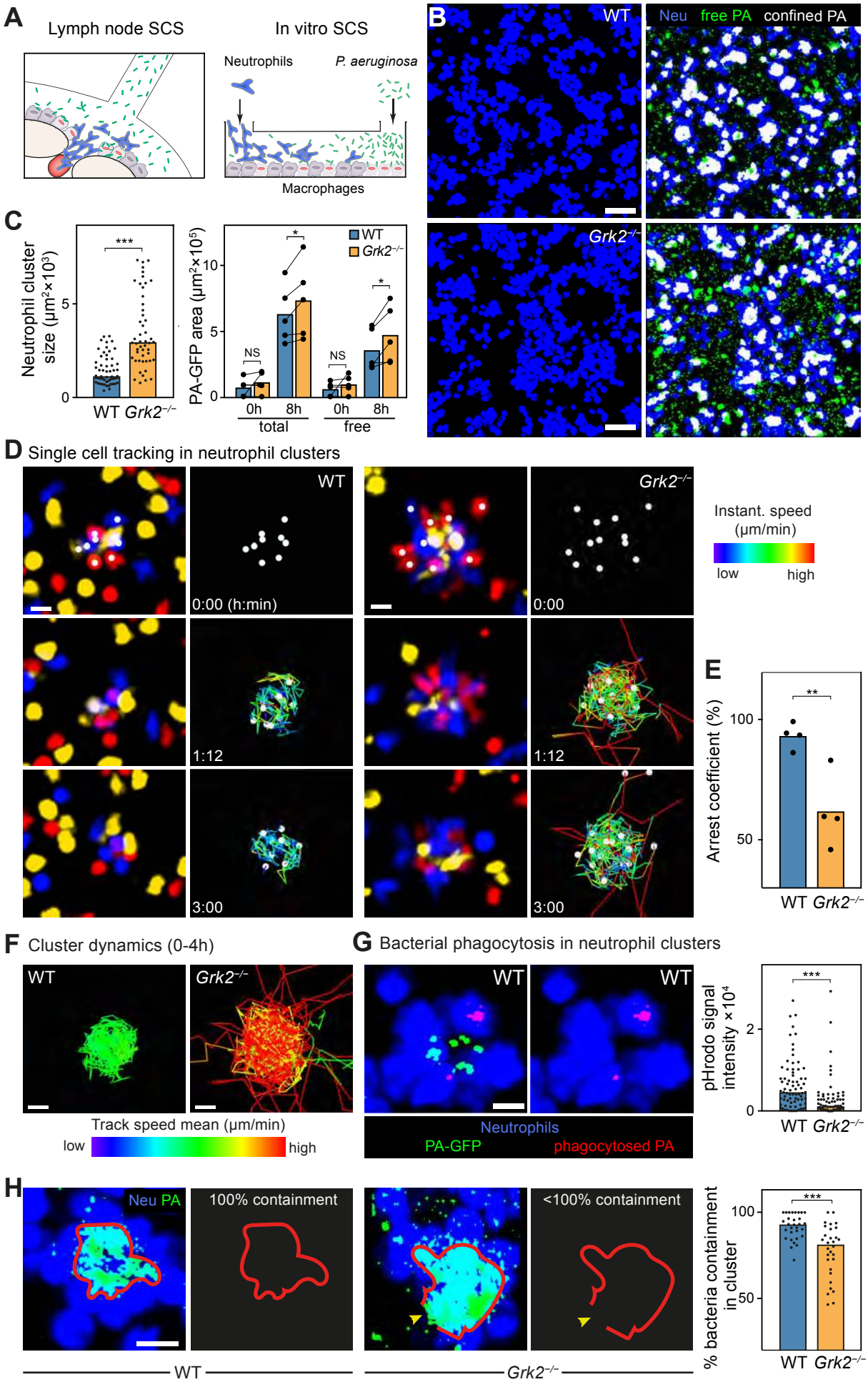
A
Lymph node SCS
In vitro SCS
Neutrophils
P. aeruginosa
Macrophages
B
WT
Neu free PA confined PA
Grk2−/−
C
Neutrophil cluster size (μm²×10³)
***
WT Grk2−/−
PA-GFP area (μm²×10⁵)
WT
Grk2−/−
*
*
NS
NS
0h 8h 0h 8h
total free
D Single cell tracking in neutrophil clusters
WT
Grk2−/−
0:00 (h:min)
0:00
1:12
1:12
3:00
3:00
Instant. speed (μm/min)
low high
E
Arrest coefficient (%)
**
100
50
WT Grk2−/−
F Cluster dynamics (0-4h)
WT
Grk2−/−
Track speed mean (μm/min)
low high
G Bacterial phagocytosis in neutrophil clusters
WT
WT
Neutrophils
PA-GFP phagocytosed PA
pHrodo signal intensity ×10⁴
***
2
0
WT Grk2−/−
H
Neu PA
100% containment
<100% containment
% bacteria containment in cluster
***
100
50
WT Grk2−/−
WT
Grk2−/−

Legends to main figures 1-4:

Fig. 1: GRK2-dependent neutrophil arrest in fields of highly concentrated swarm attractants. (**A**) Comparative analysis of wild-type (WT) and *Grk*$^{-/-}$ neutrophils migrating side by side in an under-agarose assay set-up along a combined gradient of the swarm attractants CXCL2/LTB4. *Grk*-deficient cells were lacking either an individual GRK or all four expressed GRKs (4×*Grk*$^{-/-}$). After 4 hours, migration endpoints were measured and displayed as the ratio of *Grk*$^{-/-}$ to WT mean displacement. n=3 biological replicates performed as independent experiments for each comparison, bars display the mean; NS, non-significant; **P<0.01 (post hoc after ANOVA). (**B** to **E**) Migration of WT and *Grk2*$^{-/-}$ neutrophils toward CXCL2/LTB4 was recorded with live-cell microscopy to obtain cell tracks for 3 hours. From one representative experiment, 50 cells per genotype were tracked and cell displacement and full cell tracks after 3 hours displayed (B). The same cells were analyzed for migration and chemotaxis parameters during the early phase (0–30 min) (C) and the late phase (90–180 min) (D) of movement along the attractant gradient. The velocity angle Y is the angle between the velocity vector and the y-axis (the axis of the attractant gradient), the y-straightness is the ratio of the displacement along the y-axis (Δy) to the total track length. Bars display the mean; ***P<0.001, t test (C, speed). Bars display the median; ***P<0.001, U test (C, y-straightness, and D). (E) Instantaneous velocities with representative cell shapes at t=120 min (N=50 cells per genotype, mean±s.d). (**F**) Comparative analysis of WT and *Grk2*$^{-/-}$ neutrophils migrating for 4 hours toward various attractive GPCR ligands, displayed as displacement ratio of *Grk2*$^{-/-}$ to WT cells. n=4 biological replicates performed as independent experiments for each comparison. Bars display the mean; **P<0.01, *P<0.05, NS, one sample t test against 1. (**G**) Comparative analysis of WT and *Grk2*$^{-/-}$ neutrophil mean displacement in gradients of combined LTB4 and CXCL2, or individual

attractants. *n*=4 biological replicates performed as independent experiments for each side-by-side comparison. Bars display the mean; ***P<0.001, **P<0.01, ratio paired *t* test. (**H** and **I**) Intracellular calcium-flux analysis as a measure of GPCR desensitization. WT and *Grk2*$^{-/-}$ neutrophils were stimulated sequentially with increasing concentrations of either LTB4 (H) or CXCL2 (I) (triangles, first=50 nM; second=100 nM; third=200 nM). Real-time calcium flux of one experiment representative of *n*=5–7 biological replicates for each genotype (left), and quantification of the decrease in calcium signal after repeated attractant stimulation (right). Area under the curve (AUC) of the calcium signal was measured for individual stimulation peaks. Desensitization was measured as the ratio of the second and third stimulation values to the first stimulation in each independent experiment. The distribution of AUC values around the normalized average of the first stimulation is also displayed. Bars display the mean; *n*=5–7 biological replicates for each genotype; **P<0.01, NS; *t* test. Scale bars: 500 μm (B, C, and D), and 10 μm (E).

Fig. 2: GRK2-dependent arrest in persistent swarms. (**A**) In vitro microscale array of patterned heat-killed *S. aureus* (HKSA) bioparticles (blue) to study persistent neutrophil swarms. Live microscopy of WT neutrophils (yellow) and cell tracking (pink) exemplify swarming dynamics over 3 hours. (**B**) Analysis of neutrophil aggregation in clusters of two mixed populations, quantified as WT/WT and *Grk2*$^{-/-}$/WT ratio of cells accumulating on HKSA spots (accumulation index) after 2 hours. Each dot represents one analyzed neutrophil cluster (*N*=30), pooled from *n*=3 biological replicates. Bars display the mean; ***P<0.001, *t* test. (**C** to **G**), 2P-IVM on ear dermis of anesthetized mice. Comparative analysis of persistent swarming after i.d. co-injection of WT and *Grk2*$^{-/-}$ neutrophils, which were differentially labeled with fluorescent dyes, into *Tyr*$^{c\text{-}2J/c\text{-}2J}$ (B6.Albino) mice: Interstitial cell recruitment towards a laser-induced focal

tissue injury (C). For one representative experiment, the full cell tracks toward the damage site (dotted line) over the first 40 min after the initiation of the tissue damage are displayed (D) and the cell speed analyzed (E, top). Each dot represents one tracked neutrophil (N=62) from the side-by-side comparison of WT and *Grk2*$^{-/-}$ cells in one experiment. Bars display the median; NS, non-significant, U test. (E, bottom) Comparative analysis of WT and *Grk2*$^{-/-}$ neutrophil speed during side-by-side chemotactic migration, displayed as ratio of *Grk2*$^{-/-}$ to WT; n=4 biological replicates, NS, one sample t test against 1. Neutrophil aggregation was analyzed by 2P-IVM images at the endpoint of the clustering response when neutrophil recruitment ceases (F). In the representative example (in reference to Movie S2, first part), neutrophil clustering is displayed 65 min after the initiation of tissue damage (F). Aggregation in competitive clusters of *Grk2*$^{-/-}$ and WT cells was also quantified over time (G). Accumulation index was used as a quantitative parameter for neutrophil entry into the collagen-free wound center (cyan dotted line in F), displayed as ratio of *Grk2*$^{-/-}$ to WT. Quantification began (t=0) when small aggregates have already formed, which commonly occurs 5–20 min after the initial tissue injury depending on the individual experiment. Time-courses of neutrophil clusters from n=4 biological replicates (lines) are shown. (**H**) Quantification of endpoint neutrophil clustering after i.d. co-injection of WT cells and neutrophils lacking individual GRK family members into mice. The accumulation index (ratio of *Grk*$^{-/-}$ to WT) as a measure of aggregation was calculated when neutrophil recruitment had ceased and clusters stabilized. Each dot represents one analyzed neutrophil cluster (N=4–6), pooled from n=2–3 biological replicates, ***P<0.001 (post hoc after ANOVA). (**I**) Comparative analysis of WT and *Grk2*$^{-/-}$ eosinophils forming persistent swarms around *C. elegans* dauer larvae (dotted line) in vitro. Confocal images illustrate endpoint eosinophil clusters after 2 hours. Each dot represents one analyzed eosinophil cluster (N=6–10), pooled from n=3 biological replicates, **P<0.01, t test. Scale bars: 100 µm (A and I), 50 µm (D), and 30 µm (F). Bars with

LUT color grading (F and I) display fluorescence signal intensities. SHG: second harmonic generation.

Fig. 3: GRK2-controlled transient swarming restricts bacterial growth. (**A**) Comparative analysis of sequential navigation behavior of WT and *Grk2*$^{-/-}$ neutrophils by exposing them to a first gradient of LTB4/CXCL2 (up), before adding 3 hours later a second gradient of LTB4/CXCL2 at a 90° angle (right). Cell positions after initial chemotaxis (3 hours) and reorientation (6 hours) were obtained by live-cell microscopy. (**B**) Mice were infected with bacteria in the footpad and 2P-IVM of transient neutrophil swarms was then performed on draining popliteal lymph nodes. (**C** to **E**) Mice with mixed bone marrow (*Ly6g*$^{Cre/+}$ *Rosa26*$^{LSL:Tom}$, WT, cyan; *Mrp8-Cre Grk2*$^{fl/fl}$ *Lyz2*$^{Gfp/+}$, *Grk2*$^{-/-}$, yellow) were infected with *P. aeruginosa* (PA)–GFP before endogenous neutrophils were recorded 3–5 hours later. (C) Representative time-lapse sequence of neutrophil clusters (arrows) in SCS. Below, migration tracks of neutrophils redirected to a second cluster (dotted box) with dragontails from *t*=0–30 min. (D) 2P-IVM images show a representative neutrophil cluster of a transient swarm in the infected lymph node SCS. Quantification of neutrophil accumulation in transient clusters, displayed as a ratio of *Grk2*$^{-/-}$ to WT (see also Materials and Methods). Each dot represents one cluster (*N*=16), pooled from *n*=4 infected lymph nodes, ***P<0.001, one sample *t* test against 1. (E) Trajectories of individual neutrophils are shown as tracks color-coded for mean track speed (top) of cells, which navigate in the interstitial space of lymph nodes between neutrophil clusters (bottom). The color code ranges from 2–12 µm/min. Quantification of cell track lengths over 60 min, each dot represents one tracked neutrophil (*N*=59 (WT), *N*=48 (*Grk2*$^{-/-}$)) from one experiment. (**F**) Bacterial CFU counts of draining lymph nodes 8 hours after *Grk2*$^{\Delta PMN}$ and littermate control (WT) mice were infected with *P. aeruginosa*. Each dot represents one lymph node (*N*=16),

pooled from *n*=8 mice for each genotype. (E and F) Bars display the median, ***P<0.001, *U* test. Scale bars: 1 mm (A), 50 μm (C, top, and E), and 20 μm (C, bottom, and D). SHG: second harmonic generation signal.

Fig. 4: Neutrophil arrest is critical for containing bacteria in swarm clusters. (**A**) Co-culture of neutrophils (blue), macrophages (gray) and *P. aeruginosa* PAO-1 expressing GFP (PA-GFP) (green) to mimic SCS LN infection in vitro. Red nuclei indicate dying macrophages. (**B** and **C**) WT or *Grk2*$^{-/-}$ neutrophils (Neu, blue) were separately co-cultured with macrophages and PA-GFP (green). Fluorescent macrophages are not displayed in the images (B). After 8 hours of live-cell confocal microscopy the area of individual neutrophil clusters and PA-GFP signal was analyzed (C). For neutrophil cluster size (left), bars display the median; *N*=50–55 clusters, pooled from *n*=3 biological replicates; ***P<0.001, *U* test. For PA-GFP signal (right), total bacteria are the sum of neutrophil-contained bacteria (white) and bacteria outside of cell clusters (green, free). Bars display the mean; *n*=5 biological replicates performed as independent experiments; NS, non-significant, *P<0.05, ratio paired *t* test. (**D**) Neutrophils of one genotype were triple-dye labeled to track neutrophils in cell clusters. Time sequences of representative WT (left) and *Grk2*$^{-/-}$ (right) neutrophil cluster dynamics are shown. Trajectories of individual cells are shown as dragontails over 60 min and color-coded for instantaneous speed (ranging from 0–3.6 μm/min). (**E**) Arrest coefficient (% of instantaneous speed values <2 μm/min) was used as a quantitative parameter for neutrophil stopping at clusters. Bars display the mean; each dot represents one neutrophil cluster (with >7 cells tracked in each cluster) for each genotype from *n*=4 biological replicates, **P<0.01, *t* test. (**F**) The total trajectories over 4 hours of individual cells are shown as tracks color-coded for mean track speed (ranging from 0–3.6 μm/min) in the neutrophil clusters of (D). (**G**) Example of PA-GFP phagocytosis in WT neutrophil clusters (left).

PA-GFP was tagged with pHrodo™ dye to quantify the red signal of internalized bacteria in WT or *Grk2*$^{-/-}$ neutrophil clusters (right). Dots show analyzed neutrophil clusters (*N*=74), pooled from *n*=3–4 biological replicates. Bars display the median; ***P<0.001, *U* test. (**H**) Confocal images of representative WT and *Grk2*$^{-/-}$ clusters to quantify degrees of containment (red line; continuous=100%) of PA-GFP (green) at 8 hours. Yellow arrowhead shows site of discontinuous containment. Dots show analyzed neutrophil clusters (*N*=30), pooled from *n*=3 biological replicates. Bars display the median; ***P<0.001, *U* test. Scale bars: 50 μm (B) and 10 μm (D, F, G, and H).

Captions to Main-text Movies S1-S4:

Movie S1.

***Grk2*$^{-/-}$ neutrophils continue to migrate in areas of highly concentrated swarm attractants.**

First part: WT and *Grk2*$^{-/-}$ neutrophils were differentially dye-labeled and filled in a 1:1 ratio into one well (*left*) of an under-agarose chemotaxis assay set-up. The swarm-mediating chemoattractants LTB4 (1 µM) and CXCL2 (1 µM) were filled into an opposite well to establish a gradient of increasing attractant concentrations *(highest concentration on the right)*. The representative video shows control (pseudo-colored in blue; upper panel) and *Grk2*$^{-/-}$ (pseudo-colored in orange; lower panel) neutrophils migrating toward the gradient (*left to right*). Graphic analysis of this experiment is presented in Fig. 1B to E and fig. S1F, and revealed that *Grk2*$^{-/-}$ neutrophils do not arrest, but continue to migrate at high concentrations of swarm attractants. Spinning-disk confocal microscopy (x, y = 1070 µm, 870 µm; stitched from multi-tiled images), 10 frames per second. Time is displayed as h:min. Second part: WT, *Grk2*$^{-/-}$ and 4×*Grk*$^{-/-}$ neutrophils were differentially dye-labeled and filled in a 1:1:1 ratio into one well (*left*) of an under-agarose chemotaxis assay set-up with combined LTB4/CXCL2 gradient as in the experiment before. The representative video shows control (top), *Grk2*$^{-/-}$ (middle) and 4×*Grk*$^{-/-}$ (bottom) neutrophils migrating toward the gradient (*left to right*). Graphic analysis of this experiment is presented in fig. S2F, and revealed comparable migration of 4×*Grk*$^{-/-}$ and *Grk2*$^{-/-}$ neutrophils in swarm-attractant gradients. Spinning-disk confocal microscopy (x, y = 1119 µm, 959 µm; stitched from multi-tiled images), 12 frames per second. Time is displayed as h:min.

Movie S2.

GRK2-dependent neutrophil arrest in cell clusters of persistent swarms.

First part (large neutrophil swarms): WT and *Grk2*$^{-/-}$ neutrophils were differentially dye-labeled and injected intradermally in a 1:1 ratio into the ventral ear skin of a *Tyr*$^{c\text{-}2J/c\text{-}2J}$ (B6.Albino) mouse 3 hours before laser-induced focal tissue damage (white circle at the start of the video). This representative video shows *Grk2*$^{-/-}$ (pseudo-colored in green) and control neutrophils (pseudo-colored in red) accumulating at the damage site in the skin dermis. Graphic analysis of

the recruitment phase of several experiments is presented in Fig. 2D, E, and fig. S5B and C. The analysis of the clustering response in this video is presented in Fig. 2F and G. These analyses revealed comparable recruitment of control and *Grk2*$^{-/-}$ neutrophils to the focal injury at early swarming phases. Over time, *Grk2*$^{-/-}$ neutrophils remain actively motile in growing clusters and dominate over control cells in the neutrophil cluster center. Two-photon intravital microscopy (*x*, *y*, *z* = 512 µm, 512 µm, 12 µm; merge of *z*-stack), 18 frames per second. Time is displayed in minutes. Second part (small neutrophil swarms): Primary neutrophils were isolated from the bone marrow of *Grk2*$^{\Delta PMN}$ *Lifeact-GFP* mice and injected intradermally into the ventral ear skin of a *CAG-DsRed*$^{+/+}$ *Tyr*$^{c\text{-}2J/c\text{-}2J}$ mouse 3 hours before laser-induced focal tissue damage. This representative video shows the accumulation of *Grk2*$^{-/-}$ neutrophils (pseudo-colored in green) at a small cluster of endogenous wild-type (WT) neutrophils (pseudo-colored in red) that formed at the laser damage site. The analysis of the clustering response of several experiments, including comparison to control WT *Lifeact-GFP* neutrophil injection, is presented in fig. S5E, and revealed that the continued motility of *Grk2*$^{-/-}$ neutrophils displaces control cells in the centers of small neutrophil clusters. Two-photon intravital microscopy (*x*, *y*, *z* = 512 µm, 512 µm, 3 µm; merge of *z*-stack), 24 frames per second. Time is displayed in minutes. Third part (eosinophil swarms): GRK2 controls the accumulation of swarming eosinophils around worm larvae. WT and *Grk2*$^{-/-}$ eosinophils from IL-5 cultures of WT and *Vav-iCre Grk2*$^{fl/fl}$ mouse bone marrow, respectively, were differentially dye-labeled and placed in a 1:1 ratio with 4-days old *C. elegans* dauer larvae in Matrigel. This representative video shows the recording of brightfield (top left) and fluorescent microscopy (right) in which *Grk2*$^{-/-}$ (pseudo-colored in pink) and control (pseudo-colored in blue) eosinophils swarm and accumulate side by side around an individual larva. The analysis of eosinophil clustering of several experiments is presented in Fig. 2I, and revealed an increased clustering response of *Grk2*$^{-/-}$ eosinophils at the worm larva (dotted outline). Spinning-disk confocal microscopy (*x*, *y* = 269 µm, 365 µm; stitched from multi-tiled images), 10 frames per second. Time is displayed as h:min.

Movie S3.

GRK2 controls neutrophil arrest in transient swarm clusters and limits neutrophil space exploration in infected tissues.

First part (in vitro): GRK2 limits neutrophil space exploration between competing gradients of swarm attractants. WT and *Grk2*$^{-/-}$ neutrophils were differentially dye-labeled and loaded in a 1:1 ratio into wells of a modified under-agarose assay set-up that allows the analysis of neutrophil sequential navigation behavior in response to multiple attractant sources. Neutrophils were exposed to two spatiotemporally separated gradients of the swarm attractants LTB4 (1 µM) and CXCL2 (1 µM). First, *Grk2*$^{-/-}$ (pseudo-colored in orange) and WT neutrophils (pseudo-colored in blue) respond to a first gradient of LTB4/CXCL2 (*gradient direction from top to bottom*). The movie sequence shows side-by-side migration of tracked cells and starts 2 hours after the attractants were added. Second, WT and *Grk2*$^{-/-}$ neutrophils are redirected after 3 hours by an additional second gradient of LTB4/CXCL2 at a 90° angle (*gradient direction from right to left*). This second movie starts immediately after attractants were added. Cell migration was tracked using Imaris spot function. Each circle indicates an individual neutrophil with motion paths as dragon tails over the last 10 min (first movie) or 30 min (second movie) in the corresponding pseudo-color. Graphic analysis of this video is presented in Fig. 3A and fig. S6B and C, and revealed that *Grk2*$^{-/-}$ neutrophils, in contrast to WT cells, were not desensitized by the first gradient and could be re-directed by an additional second gradient of the same attractants. Spinning-disk confocal microscopy (x, y = 1682 µm, 1391 µm; stitched from multi-tiled images), 12 frames per second. Time is displayed as h:min. Second part (*P. aeruginosa*-infected lymph node): GRK2 controls neutrophil arrest in transient swarm clusters in vivo. Mice with mixed bone marrow (*Ly6g*$^{Cre/+}$ *Rosa26*$^{LSL:Tom}$, WT, pseudo-colored in red; *Mrp8-Cre* *Grk2*$^{fl/fl}$ *Lyz2*$^{Gfp/+}$, *Grk2*$^{-/-}$, pseudo-colored in green) were injected with *P. aeruginosa* (PA)–GFP (fluorescence not visible here) into the footpad before endogenous neutrophils were recorded 3–4 hours later. Two-photon intravital microscopy of transient neutrophil swarms was performed on the subcapsular sinus of draining popliteal lymph nodes. This representative video shows *Grk2*$^{-/-}$ (pseudo-colored in green) and control neutrophils (pseudo-colored in red) side by side during the formation and disappearance of transient neutrophil swarm clusters. Arrows indicate neutrophil clusters, the pink arrow highlights neutrophil migration out of one cluster to a newly developing cluster. Static images of this video are presented in Fig. 3C. Graphic analysis of several experiments is presented in Fig. 3D and revealed that *Grk2*$^{-/-}$ neutrophils dominate over control cells in the central regions of newly forming clusters. Moreover, *Grk2*$^{-/-}$ neutrophils migrate also rapidly out of clusters again and become redirected to the centers of newly developing clusters.

Two-photon intravital microscopy (*x*, *y*, *z* = 504 µm, 404 µm, 14 µm; merge of *z*-stack), 12 frames per second. Time is displayed in minutes. Third part (*S. typhimurium*-infected lymph node): Mice with mixed bone marrow (*Ly6g*$^{Cre/+}$ *Rosa26*$^{LSL:Tom}$, WT, pseudo-colored in red; *Mrp8-Cre* *Grk2*$^{fl/fl}$ *Lyz2*$^{Gfp/+}$, *Grk2*$^{-/-}$, pseudo-colored in green) were injected with *S. typhimurium* into the footpad before endogenous neutrophils were recorded 3–4 hours later. Two-photon intravital microscopy of transient neutrophil swarms was performed on the subcapsular sinus of draining popliteal lymph nodes. This representative video shows *Grk2*$^{-/-}$ (in green) and control neutrophils (in red) side by side during the formation and disappearance of transient neutrophil swarm clusters (arrows). Static images of this video and graphic analysis of several experiments are presented in fig. S6E and F, and revealed that *Grk2*$^{-/-}$ neutrophils dominate over control cells in the central regions of newly forming clusters during *S. typhimurium* infection. Moreover, *Grk2*$^{-/-}$ neutrophils migrate also rapidly out of clusters again, have increased interstitial speed and become redirected to the centers of newly developing clusters. Two-photon intravital microscopy (*x*, *y*, *z* = 512 µm, 512 µm, 10 µm; merge of *z*-stack), 12 frames per second. Time is displayed in minutes. Fourth part (*P. aeruginosa*-infected lymph node): GRK2 limits neutrophil space exploration in infected lymph node tissue. Cell tracking of endogenous WT and *Grk2*$^{-/-}$ neutrophils that migrate side by side in the interstitial areas of a *P. aeruginosa* infected lymph node (image insert, tissue region as in second part of this video). This representative video shows the interstitial scanning behavior of *Grk2*$^{-/-}$ (pseudo-colored in green) and control neutrophils (pseudo-colored in red) with motion paths over the last 15 min as dragon tails in the corresponding pseudo-color. At the end, the total trajectories of individual neutrophils after 60 min are shown as tracks color-coded for average speed. Graphic analysis is presented in Fig. 3E and revealed that neutrophils lacking GRK2 show increased tissue scanning, but impaired migration arrest during interstitial movement in infected lymph nodes. 10 frames per second. Time is displayed in min.

Movie S4.

GRK2 controls arrest to form stable neutrophil clusters in order to contain bacterial growth.

First part**:** Swarm-like dynamics of *P. aeruginosa* precede macrophage death in vitro.

Bone marrow-derived macrophages were fluorescently labeled with CellTracker™ Blue and co-incubated with *P. aeruginosa* PAO-1 expressing GFP (PA-GFP). This representative video shows macrophages (pseudo-colored in violet) and PA-GFP (pseudo-colored in green) in the presence of propidium iodide as marker for dying cells (pseudo-colored in red), and revealed pack-swarming bacteria that precede macrophage cell death at local sites. Right panels show zoom-in on dying macrophage clusters. Static images of this video and the quantification of macrophage survival of several experiments are presented in Fig. S7B and C. Laser-scanning fluorescence confocal microscopy (x, y, z = 1024 µm, 1024 µm, 4 µm; merge of z-stack), 12 frames per second. Time is displayed in minutes. Second part: *Grk2*$^{-/-}$ neutrophils form larger clusters, but show an impaired control of bacterial growth. To mimic a bacterial infection of the lymph node subcapsular sinus in vitro, bone marrow-derived macrophages were co-incubated with PA-GFP in the presence of either *Grk2*$^{-/-}$ or WT neutrophils. This video shows representative experiments in which the swarming dynamics of WT and *Grk2*$^{-/-}$ neutrophils (pseudo-colored in blue) and bacteria (pseudo-colored in green) are shown together on the left side, and bacteria fluorescence signal alone on the right side. Macrophages were present, but are not displayed here. A graphic analysis of several experiments is presented in Fig. 4B and C, and revealed an increased growth of bacteria in experiments with *Grk2*$^{-/-}$ neutrophils in comparison to control cells, in particular in the extracellular space between neutrophil clusters. Laser-scanning fluorescence confocal microscopy (x, y, z = 513 µm, 513 µm, 4 µm; merge of z-stack), 20 frames per second. Time is displayed as h:min. Third part: GRK2 controls neutrophil arrest to form stable swarm clusters. Bone marrow-derived macrophages were co-incubated with PA-GFP in the presence of either *Grk2*$^{-/-}$ or WT neutrophils. Neutrophils of one genotype were split into three fractions and differentially labeled with three dyes (CellTracker™ Blue, 5-TAMRA, CellTracker™ Far Red), before they were pooled and added to the co-culture. The triple-color labeling allowed the identification and single cell tracking of neutrophils in dense cell clusters. This video shows representative neutrophil dynamics in one *Grk2*$^{-/-}$ or WT clusters (*left*), together with single-cell motion tracks over the last 45 min as red dragon tails and tracked cells as white circles (*right*). Graphic analysis of several experiments is presented in Fig. 4D to F and fig. S7F, and revealed that *Grk2*$^{-/-}$ neutrophils lack arrest phases at clusters and move rapidly out of them again, resulting in unstable neutrophil aggregates. Laser scanning confocal microscopy

(x, y, z = 89 µm, 78 µm, 6 µm; merge of z-stack), 15 frames per second. Time is displayed as h:min.

Science
AAAS

Supplementary Materials for

Neutrophils self-limit swarming to contain bacterial growth in vivo

Korbinian Kienle, Katharina M. Glaser, Sarah Eickhoff, Michael Mihlan, Konrad Knöpper, Eduardo Reátegui, Maximilian W. Epple, Matthias Gunzer, Ralf Baumeister, Teresa K. Tarrant, Ronald N. Germain, Daniel Irimia, Wolfgang Kastenmüller, and Tim Lämmermann

Correspondence to: laemmermann@ie-freiburg.mpg.de

This PDF file includes:

Figs. S1 to S10
Tables S1 to S4

Other Supplementary Materials for this manuscript include the following:

Main-text Movies S1 to S4
MDAR Checklist

Fig. S1.

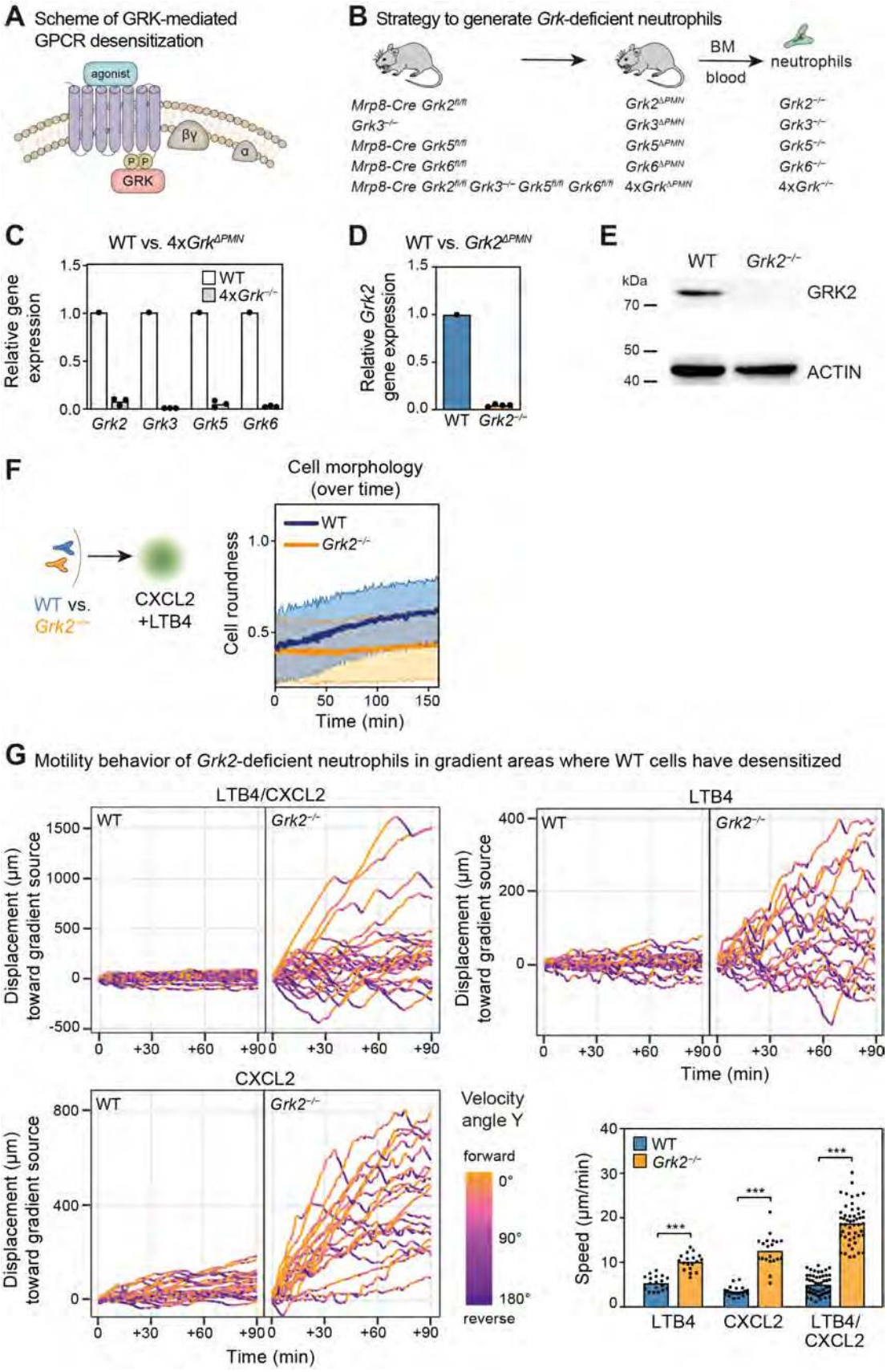
A Scheme of GRK-mediated GPCR desensitization
agonist
βγ
α
P P
GRK
B Strategy to generate Grk-deficient neutrophils
BM
blood
neutrophils
Mrp8-Cre Grk2fl/fl
Grk3−/−
Mrp8-Cre Grk5fl/fl
Mrp8-Cre Grk6fl/fl
Mrp8-Cre Grk2fl/fl Grk3−/− Grk5fl/fl Grk6fl/fl
Grk2ΔPMN
Grk3ΔPMN
Grk5ΔPMN
Grk6ΔPMN
4xGrkΔPMN
Grk2−/−
Grk3−/−
Grk5−/−
Grk6−/−
4xGrk−/−
C WT vs. 4xGrkΔPMN
Relative gene expression
WT
4xGrk−/−
Grk2 Grk3 Grk5 Grk6
D WT vs. Grk2ΔPMN
Relative Grk2 gene expression
WT Grk2−/−
E WT Grk2−/−
kDa
GRK2
ACTIN
F Cell morphology (over time)
WT vs. Grk2−/−
CXCL2 +LTB4
Cell roundness
Time (min)
G Motility behavior of Grk2-deficient neutrophils in gradient areas where WT cells have desensitized
LTB4/CXCL2
LTB4
CXCL2
Displacement (µm) toward gradient source
Time (min)
Velocity angle Y
forward
reverse
Speed (µm/min)
LTB4
CXCL2
LTB4/ CXCL2

Fig. S1: Generation of GRK-depleted primary mouse neutrophils. (**A**) The scheme illustrates the role of G-protein coupled receptor kinases (GRKs) for GPCR desensitization. GRKs can phosphorylate cytoplasmic tails of agonist-bound GPCRs, which can induce the uncoupling of G-proteins from the GPCR. This leads to the uncoupling of GPCR activation from the signaling cascade and prevents further GPCR activation. (**B**) Scheme of the breeding strategies to generate mouse models for the isolation of neutrophils lacking individual GRKs and all four neutrophil-expressed GRKs (4×*Grk*$^{-/-}$) from blood and bone marrow (BM). (**C** and **D**) Confirmation of knockout efficiency by quantitative RT-PCR. Relative gene expression in BM neutrophils isolated from 4×*Grk*$^{\Delta PMN}$ mice (C) or *Grk2*$^{\Delta PMN}$ mice (D) in comparison to wild-type (WT) littermate control mice; mean of *18S rRNA*, *B2m* and *Actb* was used to normalize gene expression, *Grk* expression levels in WT neutrophils were set to 1 (n=3–4 biological replicates, bars display mean). (**E**) Confirmation of the efficiency of conditional GRK2 knockout by immunoblot analysis of neutrophil lysates. GRK2 protein expression in BM neutrophils isolated from *Grk2*$^{\Delta PMN}$ and littermate control (WT) mice. Actin was used as loading control. (**F**) Migration of WT and *Grk2*$^{-/-}$ neutrophils toward CXCL2/LTB4 was recorded with live cell microscopy for 3 hours and cell shape was quantified over time. Roundness values closer to 1 indicate low cell polarization as observed for stopping neutrophils (mean±s.d.). Data from one experiment are shown with 50 manually tracked cells each (in reference to Fig. 1E). (**G**) Detailed analysis of the continued motility behavior of *Grk2*$^{-/-}$ neutrophils in areas of chemoattractant gradients where WT neutrophils have already desensitized and stopped movement. Displacement–time plots display the continued movement of *Grk2*$^{-/-}$ neutrophils for 90 min in gradients of combined LTB4 and CXCL2, LTB4 alone, or CXCL2 alone. Tracks are color-coded with the velocity angle Y, which displays phases of forward and reverse movement. Under all gradient conditions, *Grk2*$^{-/-}$ neutrophils continue to show net forward displacement before they reach an oscillating behavior with short alternating phases of forward and backward movement. Lower right: the measured cell speed during this 90-minute period was analyzed for gradients of LTB4 alone and CXCL2 alone. Each dot represents the mean track speed of one cell from one experiment. Bars display median; ***P<0.001, U test. These data are presented next to the data for gradients of combined LTB4 and CXCL2 (from Fig. 1D).

Fig. S2.

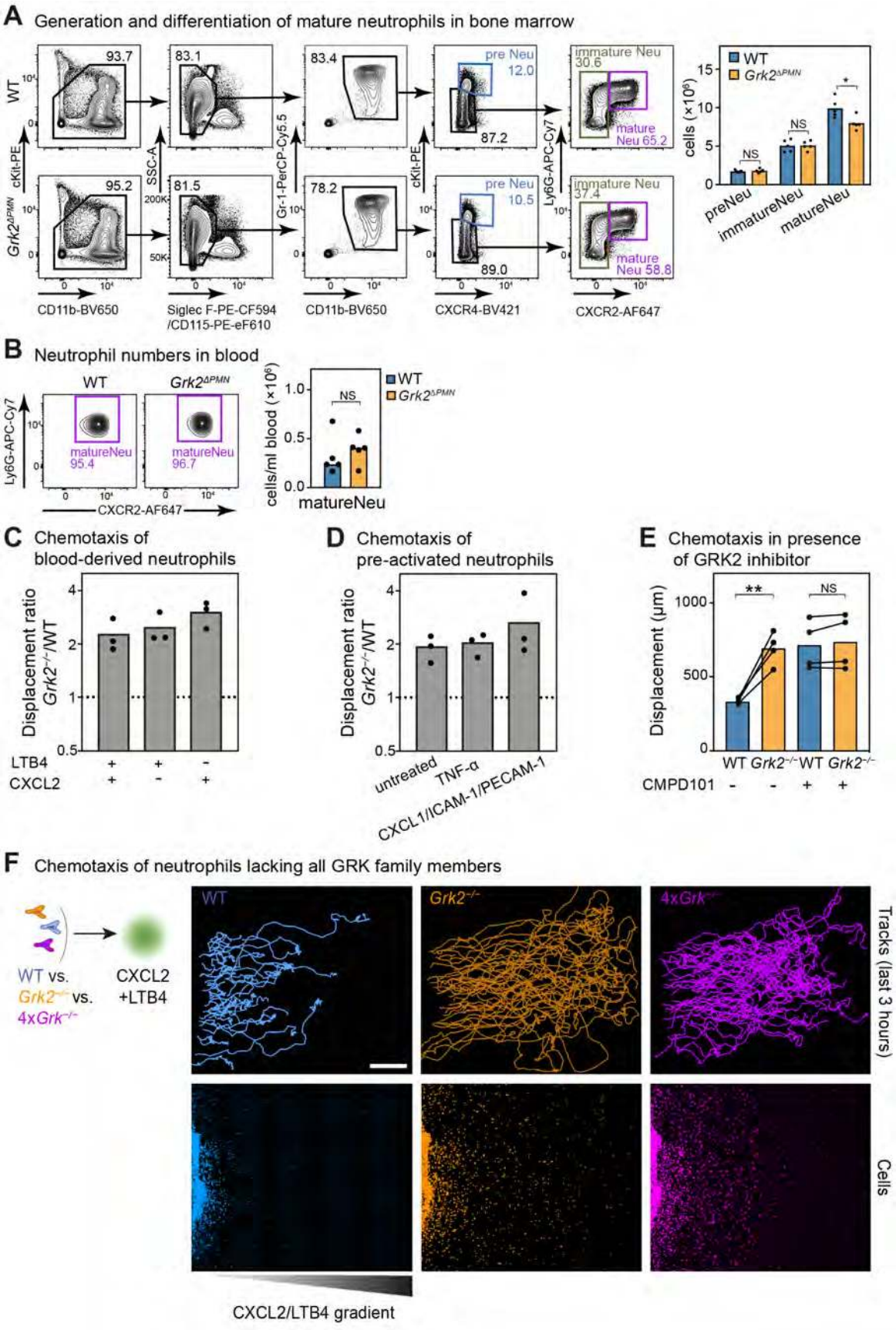
A
Generation and differentiation of mature neutrophils in bone marrow
WT
Grk2ΔPMN
cKit-PE
SSC-A
Gr-1-PerCP-Cy5.5
Ly6G-APC-Cy7
93.7
95.2
83.1
81.5
83.4
78.2
pre Neu 12.0
87.2
pre Neu 10.5
89.0
immature Neu 30.6
mature Neu 65.2
immature Neu 37.4
mature Neu 58.8
CD11b-BV650
Siglec F-PE-CF594 /CD115-PE-eF610
CD11b-BV650
CXCR4-BV421
CXCR2-AF647
cells (×10⁶)
NS
preNeu
immatureNeu
matureNeu
B
Neutrophil numbers in blood
matureNeu 95.4
matureNeu 96.7
CXCR2-AF647
cells/ml blood (×10⁶)
matureNeu
C
Chemotaxis of blood-derived neutrophils
Displacement ratio Grk2−/−/WT
LTB4
CXCL2
D
Chemotaxis of pre-activated neutrophils
untreated
TNF-α
CXCL1/ICAM-1/PECAM-1
E
Chemotaxis in presence of GRK2 inhibitor
Displacement (μm)
**
NS
CMPD101
F
Chemotaxis of neutrophils lacking all GRK family members
WT vs. Grk2−/− vs. 4xGrk−/−
CXCL2 +LTB4
Tracks (last 3 hours)
Cells
CXCL2/LTB4 gradient

Fig. S2: GRK2-dependent migration phenotype is not attributed to neutrophil origin, activation state or GRK2 inhibition strategy. (**A** and **B**) Mature neutrophils (matureNeu) are generated in the bone marrow (A) and blood (B) of WT and $Grk2^{\Delta PMN}$ mice. Left, flow cytometric analysis and gating strategy of neutrophil populations are shown. Right, (A) quantification of total neutrophil numbers in bone marrow taken from one pair of lower limbs (combined tibiae and femura) per mouse (bars display the mean; n=5 mice for each genotype, t test, NS, non-significant, *P<0.05, gating started with Lin^- cells) and (B) total numbers of mature neutrophils per milliliter blood per mouse (bars display the median, n=5 mice for each genotype, U test, NS, non-significant, gating started with Lin^- $CD115^-$ $SiglecF^-$ $Gr1^+$ $CD11b^+$ cells) were quantified. (**C** and **D**) Comparative analysis of WT and $Grk2^{-/-}$ neutrophils (C) isolated from blood, and (D) upon pre-activation (see methods for details) after 4 hours migration along a combined gradient of the swarm attractants CXCL2/LTB4. Bars display the mean, N=3 technical replicates of one experiment. **(E)** Comparative analysis of WT and $Grk2^{-/-}$ displacement after 4 hours of migration along a combined gradient of the swarm attractants CXCL2/LTB4 in the presence of the GRK2 inhibitor CMPD101. Bars display the mean; n=4 biological replicates performed as independent experiments; NS, non-significant, ratio paired t test. As comparison, data from side-by-side migration of untreated WT and $Grk2^{-/-}$ cells are displayed (from Fig. 1G). (**F**) Comparative analysis of WT, $Grk2^{-/-}$ and 4×$Grk^{-/-}$ neutrophils migrating together in the same under-agarose assay set-up toward a combined CXCL2/LTB4 gradient. Data from one representative live-cell imaging experiment are shown (in reference to Movie S1, second part). Lower row: Images display raw data of displaced cells, which have migrated for 3 hours along the gradient. Upper row: Full tracks of 50 manually tracked cells per genotype. Scale bar: 500 µm.

Fig. S3.

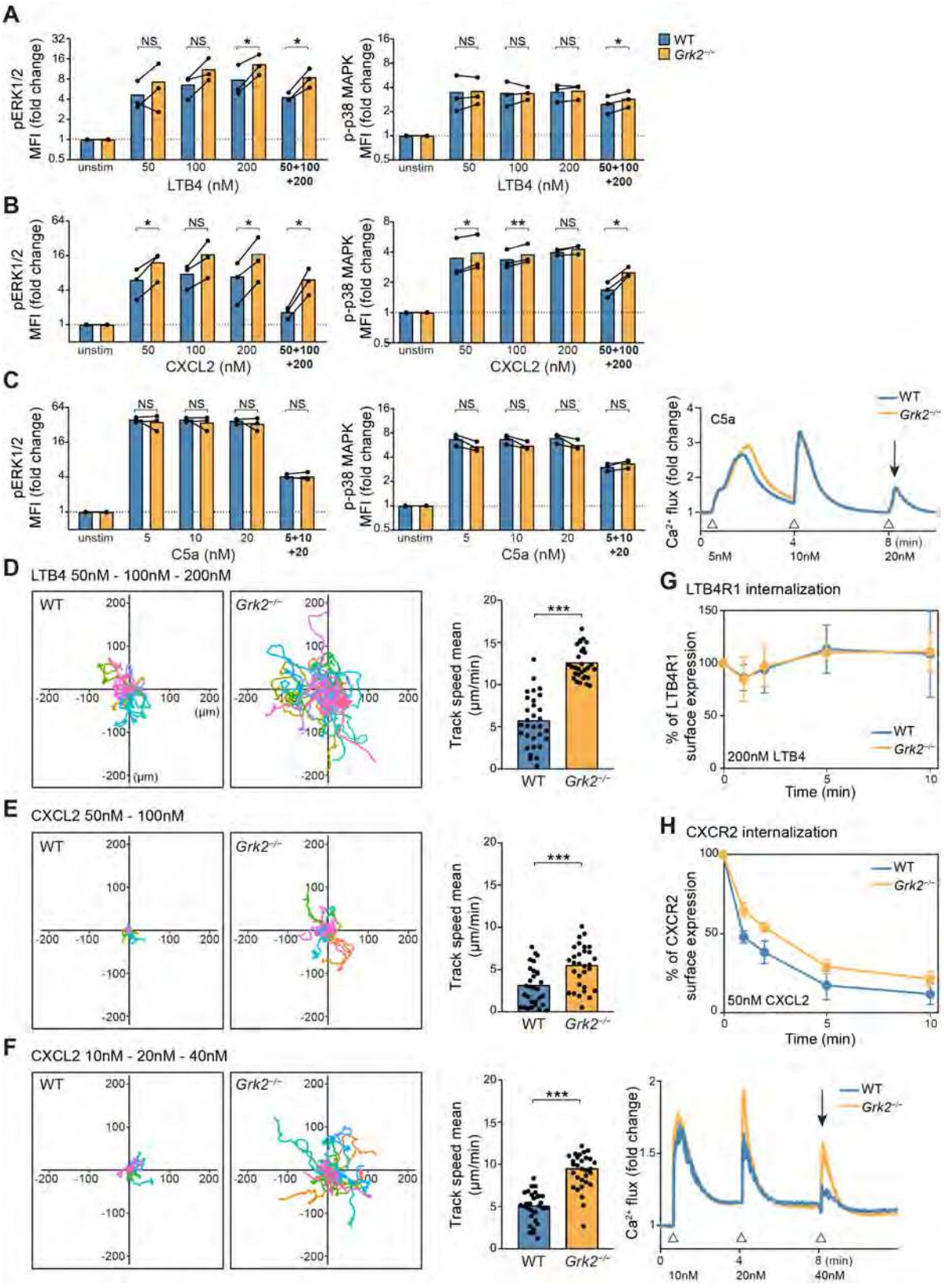
A
pERK1/2 MFI (fold change)
p-p38 MAPK MFI (fold change)
WT
Grk2−/−
NS
*
unstim
50
100
200
50+100 +200
LTB4 (nM)
B
**
CXCL2 (nM)
C
5
10
20
5+10 +20
C5a (nM)
C5a
Ca2+ flux (fold change)
5nM
10nM
20nM
8 (min)
D
LTB4 50nM - 100nM - 200nM
(μm)
Track speed mean (μm/min)
***
E
CXCL2 50nM - 100nM
F
CXCL2 10nM - 20nM - 40nM
G
LTB4R1 internalization
% of LTB4R1 surface expression
200nM LTB4
Time (min)
H
CXCR2 internalization
% of CXCR2 surface expression
50nM CXCL2
40nM

Fig. S3: Lack of GRK2 increases CXCR2 and LTB4R1 downstream signaling. (**A** and **B**) WT and *Grk2*$^{-/-}$ neutrophils were stimulated with LTB4 (A) or CXCL2 (B) and intracellular pERK1/2 (phospho-p44/p42) and p-p38 MAPK levels analyzed and quantified by flow cytometry. Neutrophils were stimulated with the attractant concentrations that were used in Fig. 1H and I to desensitize GPCR-induced calcium responses, either as individual stimulus for 2 min or stimulated sequentially with increasing concentrations (first=50 nM, second=100 nM, third=200 nM). Bars display the mean; n=3 biological replicates performed as independent experiments, *P<0.05, **P<0.01, NS, non-significant, ratio paired t test. MFI: mean fluorescence intensity. (**C**) WT and *Grk2*$^{-/-}$ neutrophils were stimulated with increasing concentrations of C5a (first=5 nM, second=10 nM, third=20 nM). Intracellular calcium-flux analysis (right) shows C5aR1 desensitization upon the third stimulation (arrow). These concentrations were applied to neutrophils as individual and sequential triple stimulations before intracellular pERK1/2 (phospho-p44/p42) and p-p38 MAPK levels were analyzed by flow cytometry. Bars display the mean; n=3 biological replicates, NS, non-significant, ratio paired t test. (**D** and **E**) WT and *Grk2*$^{-/-}$ neutrophils were stimulated with attractant concentrations that desensitize GPCR-induced calcium responses in Fig. 1H and I, and the effect on GPCR-mediated chemokinesis on ICAM-1 coated cell culture ware was recorded with live-cell microscopy over 45 min. WT and *Grk2*$^{-/-}$ neutrophils were differentially fluorescently labeled and observed side by side in the same culture well during their GPCR-mediated migration response. For LTB4 (D), neutrophils were pre-treated with triple stimulation (first=50 nM, second=100 nM, third=200 nM). For CXCL2 (E), neutrophils were pre-treated with double stimulation (first=50 nM, second=100 nM). Track lengths of N=30 cells for each genotype from one experiment were displayed (left) and mean track speed analyzed. Bars display the mean, ***P<0.001, t test. (**F**) WT and *Grk2*$^{-/-}$ neutrophils were also pre-treated with triple stimulations of CXCL2 (first=10 nM, second=20 nM, third=40 nM) that desensitized neutrophil CXCR2 at lower concentrations, as shown by intracellular calcium-flux analysis (right). Similarly pre-treated WT and *Grk2*$^{-/-}$ neutrophils were analyzed for their chemokinetic behavior. Bars display the mean, N=30 cells for each genotype from one experiment, ***P<0.001, t test. **(G** and **H)** Ligand-induced GPCR internalization was studied for WT and *Grk2*$^{-/-}$ neutrophils. Neutrophils were stimulated with 200 nM LTB4 (G) or 50 nM CXCL2 (H) to study the internalization of LTB4R1 or CXCR2, respectively, over several time points. Values are mean ± s.d. from n=3 (LTB4) and n=2 (CXCL2) biological replicates performed as independent experiments.

Fig. S4.

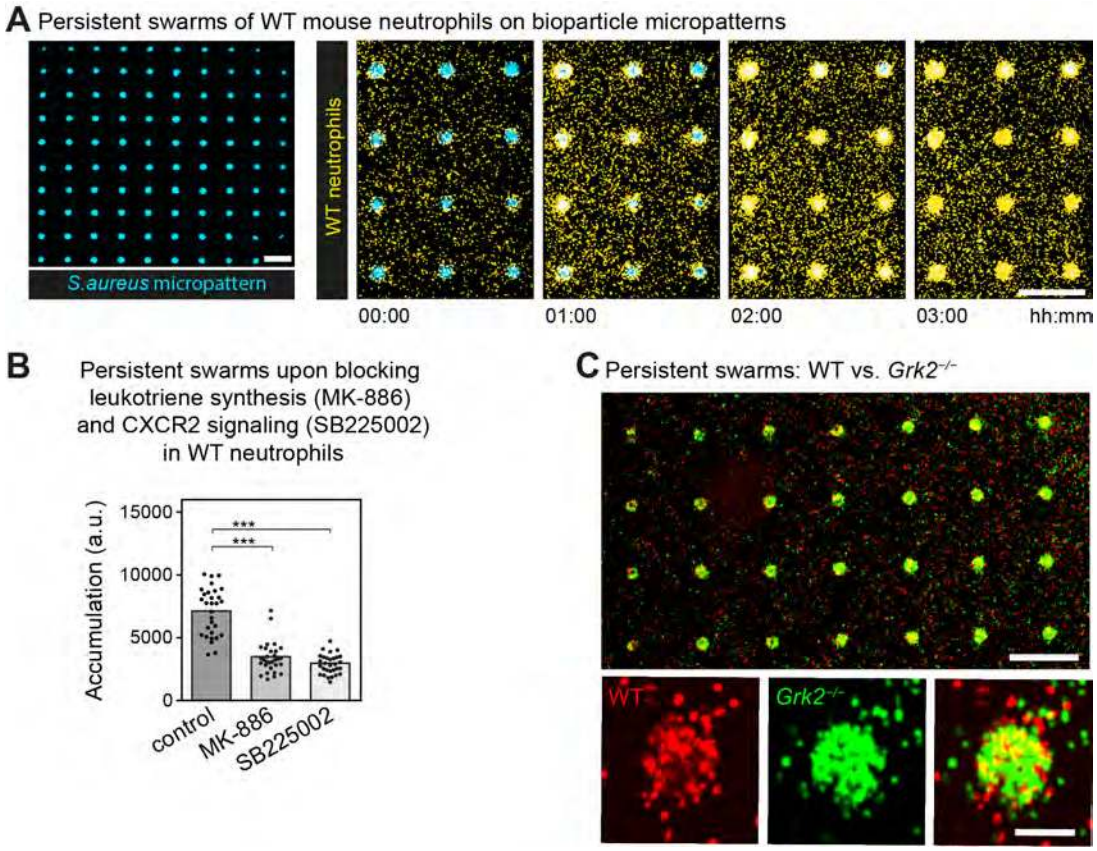

Fig. S4: GRK2-controlled persistent neutrophil swarming in vitro. (**A**) Left: representative profile of a microarray slide patterned with clusters of heat-killed *S. aureus* bioparticles (blue, 130-µm diameter, ca. 400-µm spacing between clusters) used for live-cell confocal microscopy of neutrophil persistent swarms in vitro (as used in Fig. 2A and B). Right: time-lapse sequence over 3 hours of mouse WT BM neutrophils (yellow) that swarm and aggregate on micropatterns. Scale bars: 500 µm. (**B**) Confirmation of LTB4- and CXCL2-dependence for mouse neutrophil swarming, as previously shown for human neutrophils in this in vitro assay (*12*). Quantification of neutrophil accumulation on bioparticle patterns in the presence of 10 µM MK886 (inhibitor for 5-lipoxygenase-activating protein and thus 5-lipoxygenase activity), 50 µM SB225002 (CXCR2 antagonist), or left untreated, after 2 hours. Each data point indicates one neutrophil cluster, N=30 clusters per condition, pooled from n=3 biological replicates performed as independent experiments. ***P<0.001 (post hoc after ANOVA). (**C**) Representative confocal images of competitive neutrophil aggregation in mixed *Grk2*$^{-/-}$/WT clusters on micropatterns (t=2 hours) (quantified in Fig. 2B). Scale bars: 500 µm (overview), and 100 µm (single cluster).

Fig. S5.

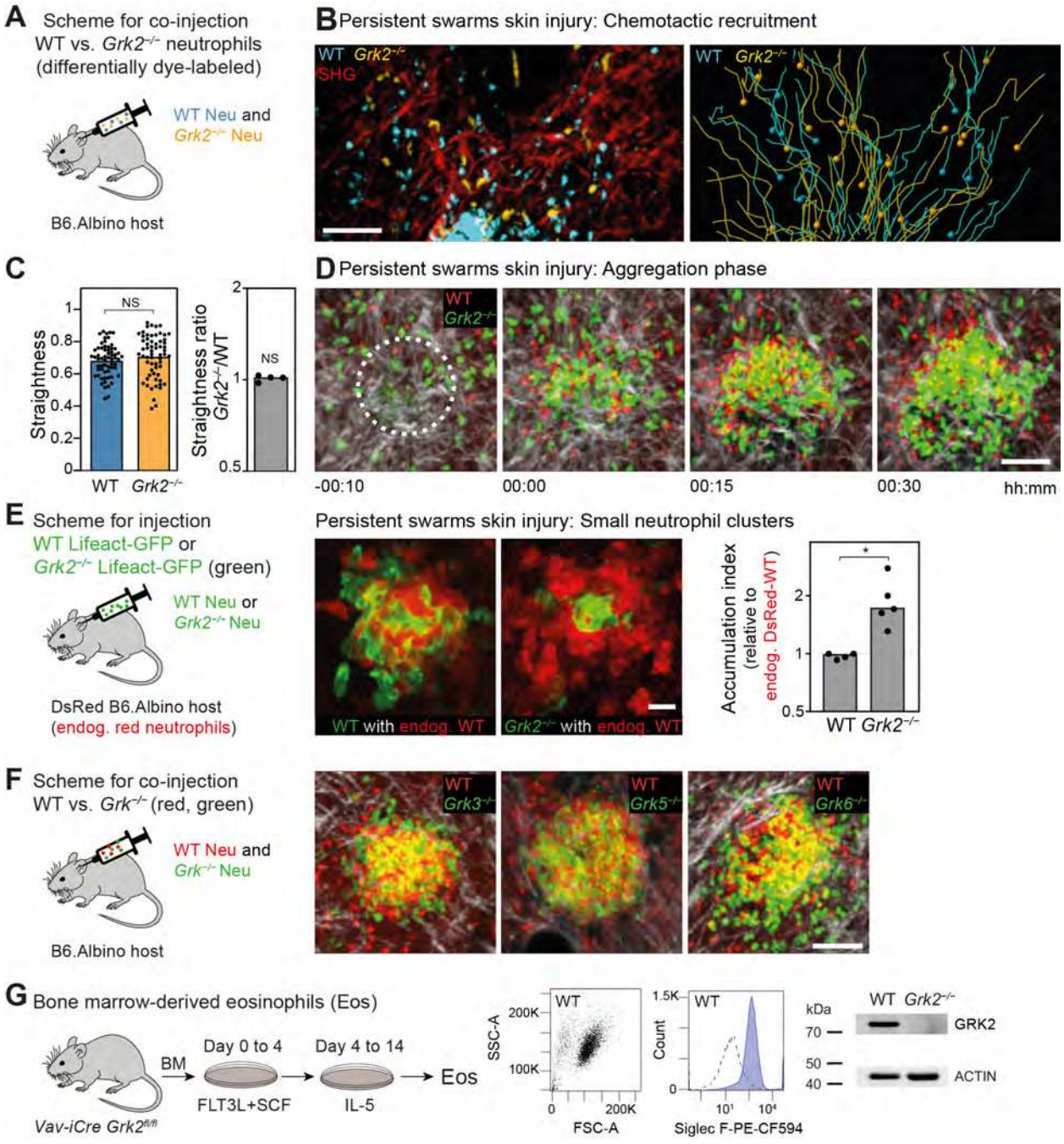

Fig. S5: GRK2, but not other GRK, controls arrest in persistent swarms. (**A**) Scheme for the comparative analysis of WT and *Grk2*$^{-/-}$ neutrophils in persistent swarms in vivo. Differentially dye-labeled WT and *Grk2*$^{-/-}$ BM neutrophils were co-injected into the ear dermis of *Tyr*$^{c\text{-}2J/c\text{-}2J}$ (B6.Albino) recipient mice. Afterwards, focal laser damage was induced in the ear dermis and the neutrophil swarming response recorded with two-photon intravital microscopy (2P-IVM) (see Fig. 2C). (**B**) In reference to Fig. 2D, a raw data image of the dermal skin area and side-by-side visualization of the cell tracks are shown and used for the quantification in Fig. 2E and fig. S5C.

(**C**) For the representative experiment in Fig. 2D and fig. S5B, the straightness of neutrophil chemotactic migration toward a developing neutrophil cluster was analyzed (left). Each dot represents one cell (N=62 for each genotype) from one experiment. Bars display the median; NS, non-significant, U test. Comparative analysis of WT and *Grk2*$^{-/-}$ neutrophil straightness during side-by-side chemotactic migration, displayed as ratio of *Grk2*$^{-/-}$ to WT for n=4 biological replicates (right); NS, one sample t test against 1. (**D**) Representative time sequence of one developing mixed *Grk2*$^{-/-}$/WT neutrophil cluster recorded by 2P-IVM (in reference to Fig. 2 G). The white dotted line indicates the area of focal skin injury. White signal shows second harmonic generation signals of dermal collagen fibers. (**E**) 2P-IVM analysis of small neutrophil clusters in vivo. Control mice and GRK2-deficient mice were intercrossed with Lifeact-GFP transgenic mice to isolate BM neutrophils with green fluorescent actin cortex. WT or *Grk2*$^{-/-}$ neutrophils (pseudo-colored in green) were injected i.d. into *DsRed*$^{+/+}$ *Tyr*$^{c\text{-}2J/c\text{-}2J}$ (B6.Albino) mice, which ubiquitously express DsRed protein in all cells. This strategy allowed the competitive analysis of WT or *Grk2*$^{-/-}$ BM neutrophils with endogenous WT neutrophils (red) in clusters. Middle: representative 2P-IVM images at the endpoint of the clustering response. Right: accumulation index (Green cell/Red cell ratio) was used as quantitative parameter for neutrophil entry into the cluster center. Each dot represents one analyzed neutrophil cluster, data from two mice per genotype. Bars display the median; *P<0.05, U test. (**F**) As shown above (A), differentially dye-labeled WT and GRK-deficient (*Grk3*$^{-/-}$, *Grk5*$^{-/-}$, *Grk6*$^{-/-}$) BM neutrophils were co-injected i.d. into the ear dermis of *Tyr*$^{c\text{-}2J/c\text{-}2J}$ recipient mice before laser damage induction. Representative 2P-IVM images at clustering endpoints are shown (quantification in Fig. 2H). Scale bars: 50 μm (C, D, and F), and 10 μm (E). (**G**) Left: scheme of bone marrow (BM)-derived eosinophil culture. Middle: representative flow cytometric plots of eosinophil in vitro differentiation at day 14. Right: confirmation of the efficiency of conditional GRK2 knockout by immunoblot analysis of eosinophil (day 14) lysates. GRK2 protein expression in BM eosinophils generated from the BM of *Vav-iCre Grk2*$^{fl/fl}$ mice and littermate Cre-negative control (WT) mice. Actin was used as loading control.

Fig. S6.

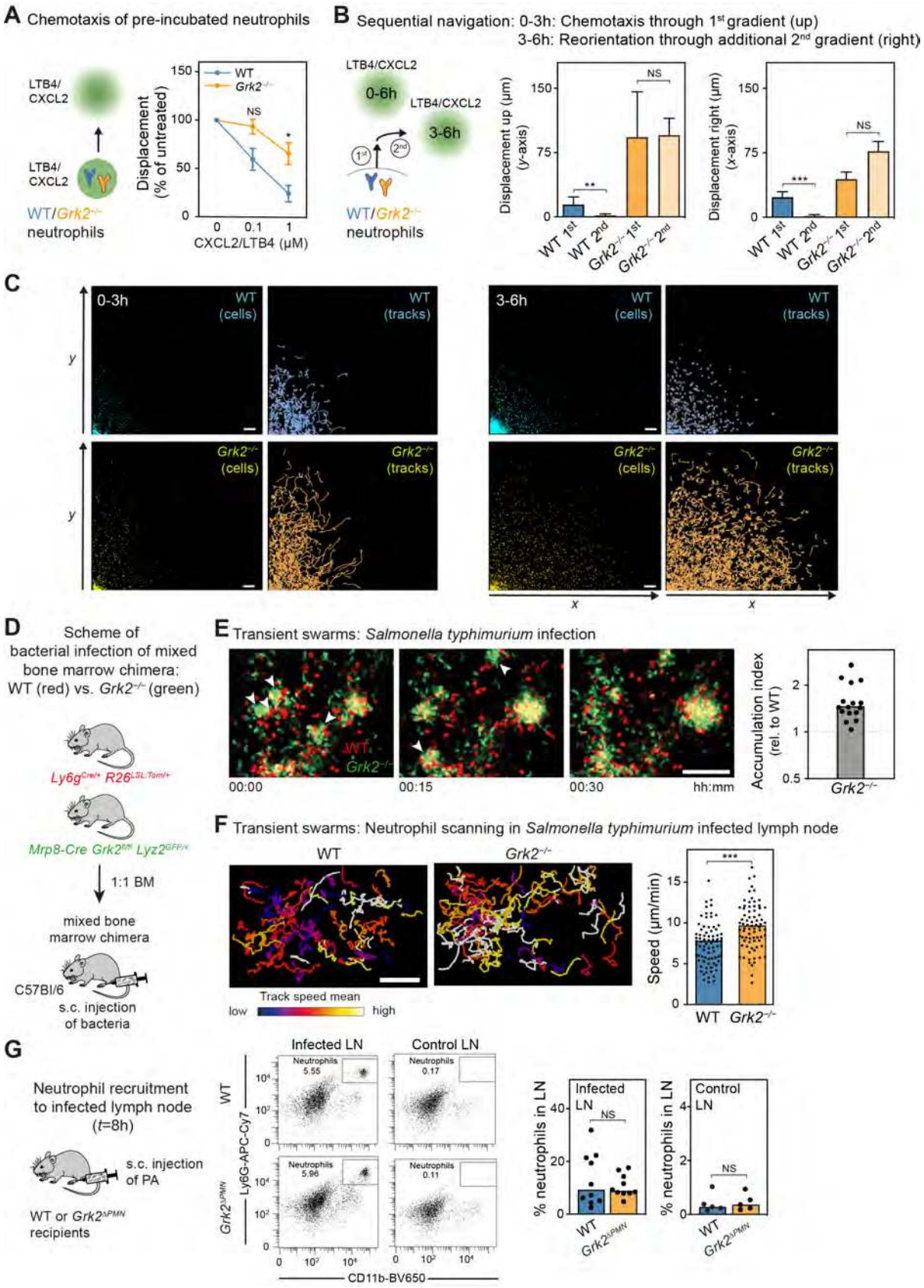
A Chemotaxis of pre-incubated neutrophils
LTB4/ CXCL2
LTB4/ CXCL2
WT/Grk2−/− neutrophils
Displacement (% of untreated)
WT
Grk2−/−
NS
CXCL2/LTB4 (μM)
B Sequential navigation: 0-3h: Chemotaxis through 1st gradient (up)
3-6h: Reorientation through additional 2nd gradient (right)
LTB4/CXCL2
0-6h
LTB4/CXCL2
3-6h
WT/Grk2−/− neutrophils
Displacement up (μm) (y-axis)
Displacement right (μm) (x-axis)
NS
WT 1st
WT 2nd
Grk2−/− 1st
Grk2−/− 2nd
C
0-3h
3-6h
WT (cells)
WT (tracks)
Grk2−/− (cells)
Grk2−/− (tracks)
y
x
D Scheme of bacterial infection of mixed bone marrow chimera: WT (red) vs. Grk2−/− (green)
Ly6gCre/+ R26LSL-Tom/+
Mrp8-Cre Grk2fl/fl Lyz2GFP/+
1:1 BM
mixed bone marrow chimera
C57Bl/6
s.c. injection of bacteria
E Transient swarms: Salmonella typhimurium infection
WT
Grk2−/−
00:00
00:15
00:30
hh:mm
Accumulation index (rel. to WT)
F Transient swarms: Neutrophil scanning in Salmonella typhimurium infected lymph node
WT
Grk2−/−
Track speed mean
low
high
Speed (μm/min)
G
Neutrophil recruitment to infected lymph node (t=8h)
s.c. injection of PA
WT or Grk2ΔPMN recipients
Infected LN
Control LN
Neutrophils 5.55
Neutrophils 0.17
Neutrophils 5.96
Neutrophils 0.11
Ly6G-APC-Cy7
CD11b-BV650
% neutrophils in LN
Infected LN
Control LN
NS

Fig. S6: GRK2 controls sequential navigation and transient swarming *in vivo*. (**A**) Analysis of neutrophil migration behavior in the presence of several attractant sources. WT and *Grk2*$^{-/-}$ neutrophils were pre-incubated with increasing concentrations of combined CXCL2/LTB4 (0, 0.1, and 1 μM for both attractants) before their chemotactic migration toward a combined CXCL2/LTB4 gradient (1 μM for both attractants) was analyzed for 4 hours. Cell displacement after chemoattractant pre-incubation was quantified relative to displacement of untreated cells (mean ± SEM, *n*=3 biological replicates performed as independent experiments, *t* test, NS, non-significant, **P*<0.05). (**B**) Quantification of neutrophil sequential navigation in response to two spatiotemporally separated CXCL2/LTB4 gradients (in reference to Fig. 3A). Cell displacement after initial chemotaxis toward the first gradient (along y-axis, for 3 hours) and after reorientation toward the second gradient (along *x*-axis, for the following 3 hours) were measured from one representative experiment (median with 95% CI, confidence interval; 0–3 hours: *N*(WT)=344 tracks, *N*(*Grk2*$^{-/-}$)=156 tracks; 3–6 hours: *N*(WT)=396 tracks, *N*(*Grk2*$^{-/-}$)=820 tracks; NS, non-significant, ***P*<0.01), ****P*<0.001 (post hoc after Kruskal–Wallis). (**C**) In reference to Fig. 3A and Movie S3 (first part), raw data images and cell tracks of sequential navigation in an under-agarose set-up are shown. These data build the basis for the quantification in fig. S6B. **(D)** To image endogenous WT and *Grk2*$^{-/-}$ neutrophils side by side in bacteria-infected lymph nodes, C57BL/6 mice were lethally irradiated and reconstituted with bone marrow from *Ly6g*$^{Cre/+}$ *Rosa26*$^{LSL:Tom}$ (WT, neutrophils red) and *Mrp8-Cre Grk2*$^{fl/fl}$ *Lyz2*$^{Gfp/+}$ (*Grk2*$^{-/-}$, neutrophils bright green) mice at a 1:1 ratio. Eight to ten weeks after BM reconstitution, bone marrow chimeric mice were infected with bacteria by subcutaneous injection in the footpad. Neutrophil dynamics in the subcapsular sinus (SCS) of popliteal draining lymph nodes were recorded 3–5 hours later by 2P-IVM. (**E**) Representative 2P-IVM time-lapse sequence of transient neutrophil swarm formation in SCS of mice infected with *Salmonella typhimurium* (ST) (in reference to Movie S3, third part). Left: white arrowheads in the image sequence highlight transient neutrophil swarms and clusters. Right: accumulation index (*Grk2*$^{-/-}$ (green)/WT (red) ratio) was used as quantitative parameter for neutrophil entry into the cluster center. Each dot represents one analyzed neutrophil cluster (*N*=16), pooled from *n*=4 biological replicates. (**F**) Tracking of WT and *Grk2*$^{-/-}$ neutrophils migrating side-by-side in ST-infected lymph nodes. Trajectories of individual neutrophils over 35 min are shown as tracks color-coded for mean track speed (left), the mean speed of single neutrophils was analyzed and compared (right). Each dot represents one tracked neutrophil (*N*=80 cells for each genotype) from one experiment. Bars display the median; ****P*<0.001, *U* test. (**G**) *Grk2*$^{\Delta PMN}$ and littermate control (WT) mice were infected s.c. with *P. aeruginosa* (PA) (left). After 8 hours, cervical (control) and draining popliteal (infected) lymph nodes were isolated, homogenized, and Ly6g^{+}/CD11b^{+} neutrophil recruitment measured by flow cytometry. Representative flow cytometric profiles are shown for individual lymph nodes (middle). Comparative analysis of neutrophil numbers relative to total cells in lymph nodes (right) (*N*=10 infected popliteal lymph nodes from *n*=5 mice; bars display the median; *U* test, NS, non-significant). Scale bars: 300 μm (C) and 100 μm (E and F).

Fig. S7.

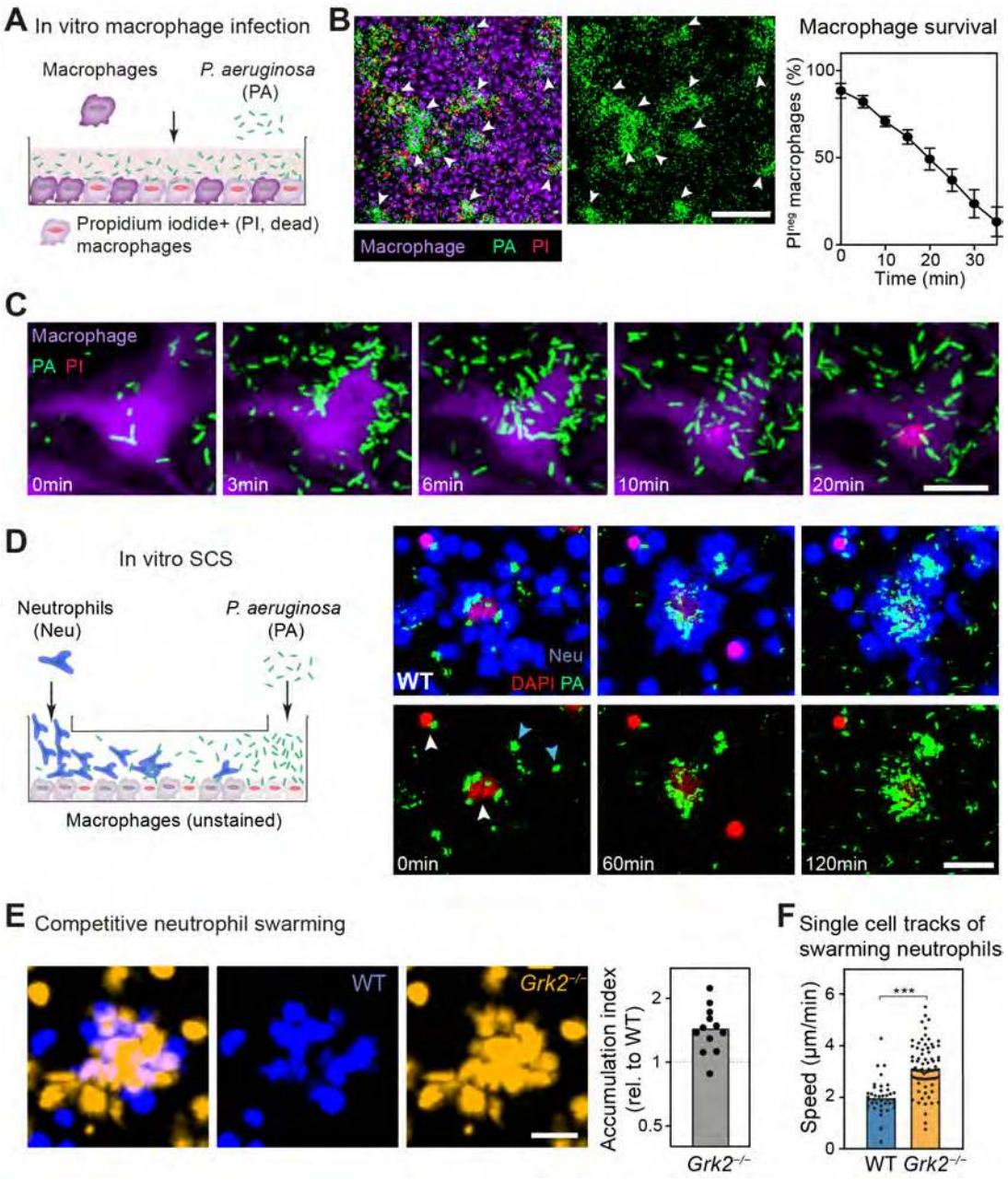

Fig. S7: Neutrophil swarming in an in vitro mimic of a bacteria-infected subcapsular sinus. (**A**) Macrophages (purple) were infected with *P. aeruginosa* PAO1-GFP (PA-GFP, pseudo-colored in green) to mimic the initial events in the lymph node SCS when bacteria infect macrophages and cause their death in the absence of neutrophils. Propidium iodide (PI, red) was used as marker for dying cells. (**B**) Left, confocal overview images of macrophage cultures (pseudo-colored in purple) that were infected with PA-GFP (pseudo-colored in green). White arrowheads highlight bacteria clusters that form in a swarm-like fashion and precede macrophage cell death at local sites (in reference to Movie S4, first part). Right, the decrease in macrophage survival (the percentage of PI-negative cells in one imaging field of view) after PA infection was measured and analyzed over time (*N*=4 technical replicates from one experiment, mean ± s.d.).

(**C**) Time-lapse sequence of a representative example showing the swarm-like accumulation of PA bacteria preceding the death of the infected macrophage (in reference to Movie S4, first part). (**D**) Experimental in vitro co-culture setup to mimic later phases of lymph node SCS infection. Neutrophils (pseudo-colored in blue) and PA-GFP (pseudo-colored green) were added to macrophages through separate ports (see details in methods section). Confocal images show a time-lapse sequence of neutrophil clusters that develop around foci of dead cells (neutrophils and macrophages) with bacteria (white arrowheads) and around aggregates of proliferating bacteria alone (cyan arrowheads). DAPI (pseudo-colored in red) was used as marker for dying cells. (**E**) Representative confocal images of mixed clusters of WT (pseudo-colored in blue) and *Grk2*$^{-/-}$ (pseudo-colored in yellow) neutrophils in the in vitro co-culture model (macrophages and bacteria are present, but not labeled). The accumulation index (ratio of *Grk2*$^{-/-}$ to WT) was used as quantitative parameter for neutrophil accumulation in the cluster center. Each dot represents a neutrophil cluster (N=12), pooled from n=3 biological replicates. (**F**) Comparative analysis of the mean speed of neutrophils that were tracked in WT and *Grk2*$^{-/-}$ cell clusters (in reference to Fig. 4E). Each dot represents one tracked neutrophil (N=38, pooled from n=4 WT neutrophil clusters; N=75 from n=4 *Grk2*$^{-/-}$ neutrophil clusters). Bar graphs display the median; U test, ***P<0.001. Scale bars: 200 μm (B), 20 μm (C and E), and 25 μm (D).

Fig. S8.

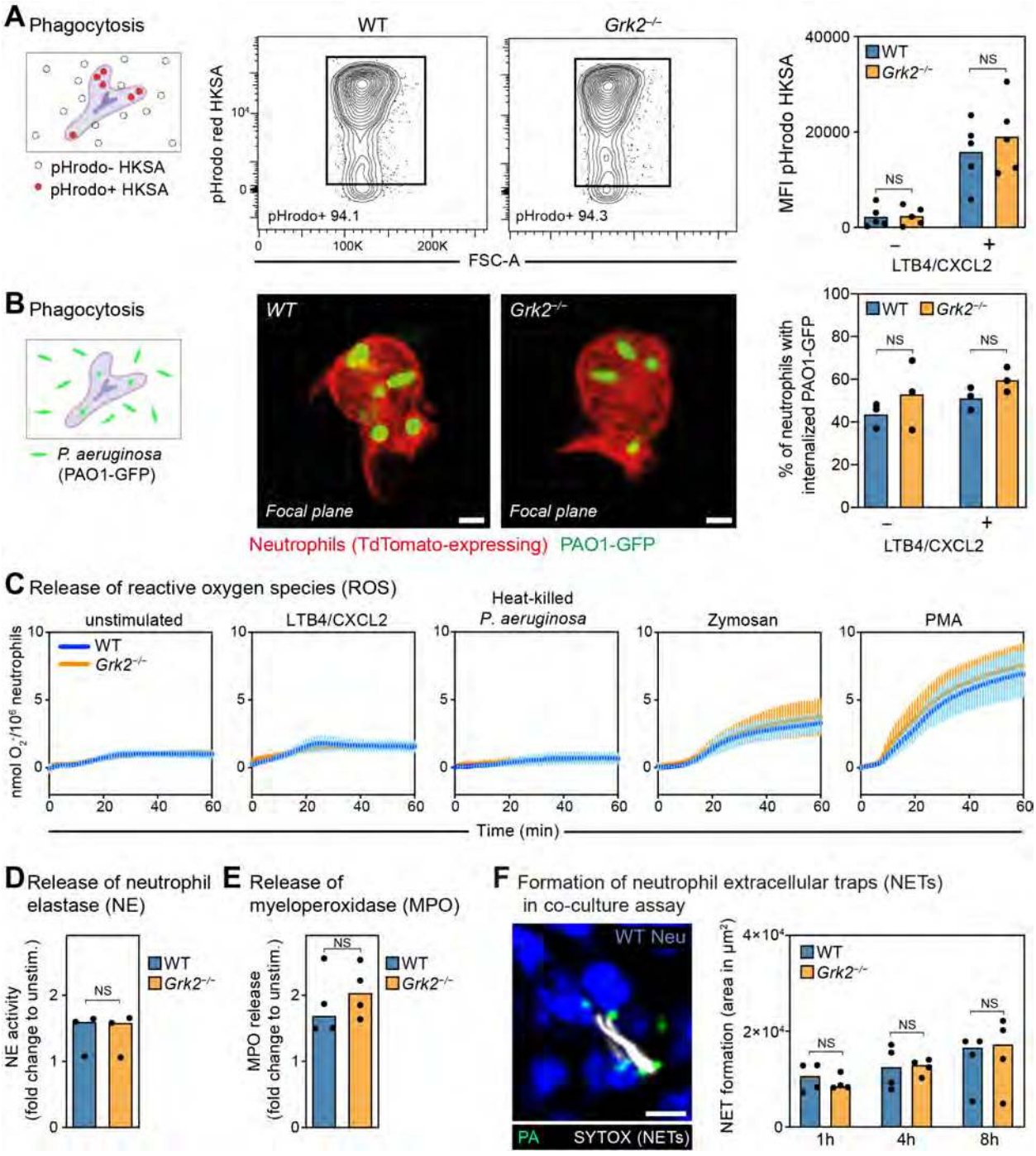

Fig. S8: *Grk2*$^{-/-}$ and WT neutrophils have no measurable differences in neutrophil effector functions. (**A**) As standard measure for neutrophil phagocytotic activity, neutrophils were co-incubated with pHrodo^{TM}-labeled heat-killed *S. aureus* bioparticles (pHrodo HKSA) and uptake analyzed by flow cytometry. Representative flow cytometric plots show phagocytosis of HKSA-pHrodo^{TM} bioparticles over 2 hours in the presence of LTB4/CXCL2 (100 nM each) (middle). Quantification of HKSA uptake is shown on the right. Bar graphs display the mean, *n*=5

biological replicates, *t* test, NS, non-significant. (**B**) TdTomato-expressing neutrophils from either WT mice (*Mrp8-Cre Grk2*$^{+/+}$ *R26*$^{LSL:Tom}$) or *Grk2*$^{\Delta PMN}$ mice (*Mrp8-Cre Grk2*$^{fl/fl}$ *R26*$^{LSL:Tom}$) were co-incubated with living *P. aeruginosa* PAO1-GFP at MOI=20 for 1 hour under continuous shaking. Bacterial phagocytosis occurred in the absence or presence of LTB4/CXCL2 (100 nM each), and bacterial internalization was determined by microscopic image analysis of non-fixed cells. Representative confocal microscopy images of WT and *Grk2*$^{-/-}$ neutrophils with internalized PAO1-GFP are displayed (scale bar: 2 µm). Quantification of PAO1-GFP uptake is shown on the right. Bar graphs display the mean, *n*=3 biological replicates; NS, non-significant, *t* test. (**C**) Real-time measurements of reactive oxygen species (ROS) release after WT and *Grk2*$^{-/-}$ neutrophils were treated with various stimuli: LTB4 and CXCL2 (100 nM of each attractant), heat-killed *Pseudomonas aeruginosa* (HKPA) particles (100 particles per one cell), zymosan (10 µg/ml), PMA (10 nM), or left untreated (mean ± s.d, *n*=3 biological replicates). (**D** and **E**) Comparative analysis of neutrophil elastase (NE) (D) and myeloperoxidase (MPO) (E) release after WT and *Grk2*$^{-/-}$ neutrophils were stimulated for 2 hours with LTB4/CXCL2 (100 nM each). NE and MPO release of stimulated cells are displayed as fold change to unstimulated cells. Bar graphs display the median, *n*=3-4 biological replicates, *U* test, NS, non-significant. (**F**) Neutrophil extracellular trap (NET) formation was analyzed in the in vitro co-culture assay (see fig. S7D). Macrophages, neutrophils (pseudo-colored in blue) and bacteria (pseudo-colored in green) were co-cultured in the presence of SYTOX^{TM} orange dye as marker for extracellular DNA. Left, NETs were identified as decondensed, extracellular SYTOX^{TM} orange-positive structures (pseudo-colored in white) and quantified using NET fluorescence signal area. Only occasional NET formation was observed in this co-culture assay. Scale bar: 20 µm. Right, quantification of NET release over time is displayed (median, *n*=4 biological replicates).

Fig. S9.

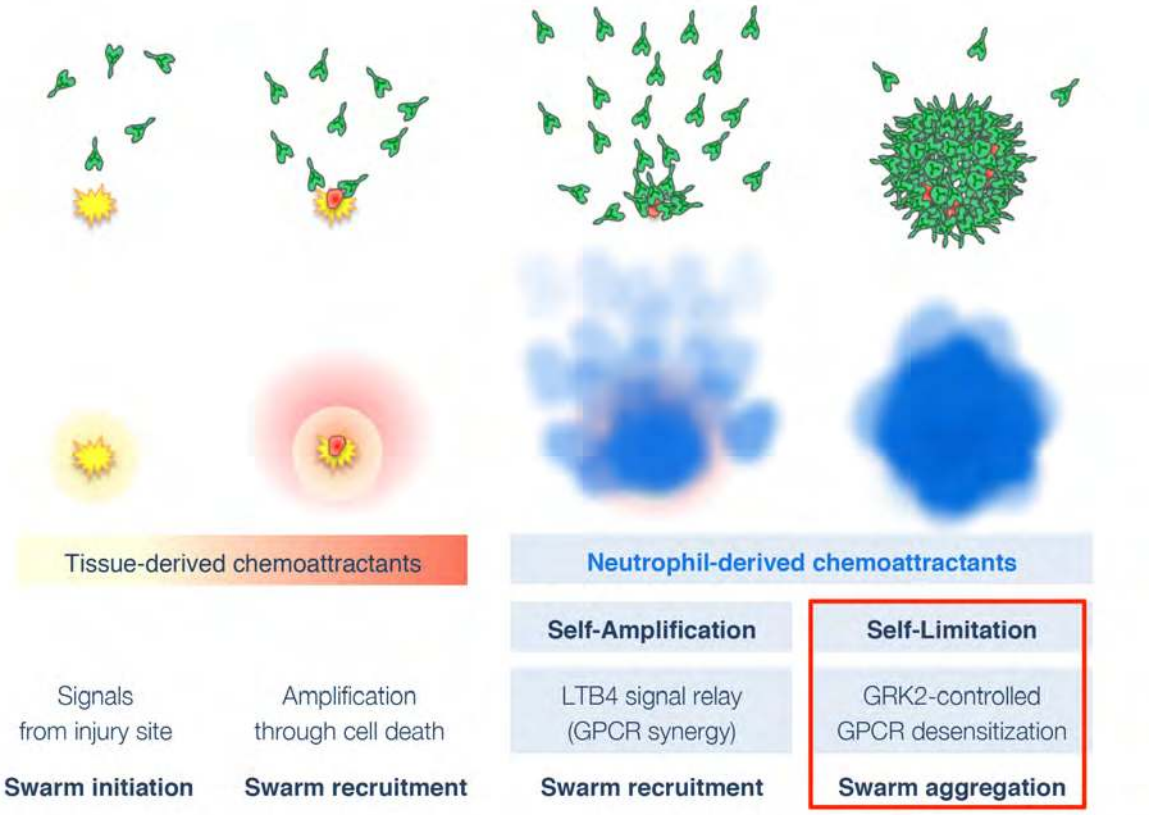

Fig. S9: Scheme of the sequential phases controlling neutrophil swarming in mice. Upon local tissue wounding, sentinel neutrophils close to the injury site sense chemotactic factors (yellow) released from damaged tissue. Cell death events (e.g. through pathogens that cause secondary cell death) release additional tissue-derived signals (red), which recruit neutrophils and often amplify neutrophil recruitment. The molecular players mediating these early phases of neutrophil swarm initiation have not yet been well characterized in mammalian tissues. Tissue-derived factors trigger the release of neutrophil-derived chemoattractants (blue), in particular leukotriene B4, which acts as a signal relay molecule and acute signal to self-amplify neutrophil recruitment from distant tissue sites. In this study we show that neutrophils have an intrinsic mechanism to self-limit their swarming behavior. In growing swarm aggregates, neutrophils sense high concentrations of accumulating swarm-secreted chemoattractants (LTB4 and CXCL2), which leads to the GRK2-controlled desensitization of the corresponding G protein-coupled receptors (GPCR) and the limitation of further swarming.

Fig. S10.

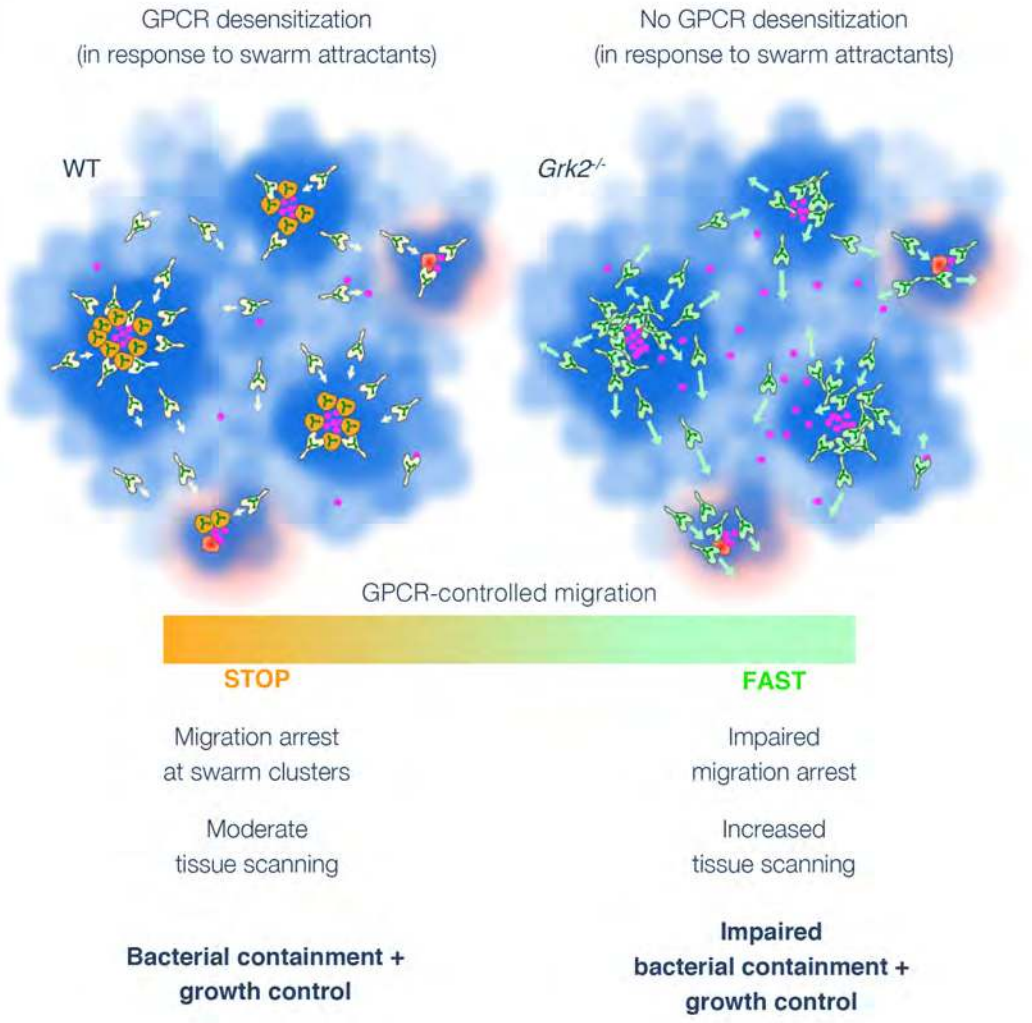

Fig. S10: Scheme of the finely tuned balance of GPCR-controlled chemotaxis and arrest in swarming neutrophils to counteract bacterial growth in infected tissues. Bacteria-induced macrophage death recruits large numbers of neutrophils from the blood to the subcapsular sinus of infected lymph nodes. Neutrophils perform transient swarming and accumulate at multiple sites where cell death (e.g. macrophages) and/or bacteria proliferation occurs. GPCR-controlled swarming dynamics depend on neutrophil-secreted attractants (blue), in particular LTB4 (*9*). Accumulating neutrophils can be redirected through competing attractant gradients from bigger neutrophil clusters (blue) or from novel sites of cell death (red). (Left) High local concentrations of swarm attractants (LTB4 and CXCL2) cause desensitization of the respective GPCRs in WT neutrophils. Neutrophils then arrest and form stable neutrophil clusters to contain proliferating bacteria (purple). (Right) *Grk2*-deficient neutrophils are lacking GPCR desensitization in response to swarm attractants, resulting in increased swarming and tissue scanning. The impaired migration arrest leads to unstable neutrophil clusters and impaired phagocytosis in clusters, allowing the escape of bacteria.

Table S1.

Table S1 lists all mouse strains used in this study.

Mouse strain	Symbol	Source
Grk2$^{fl/fl}$	Grk2^{tm1Gwd}	012458, Jackson Laboratories, Bar Harbor, ME
Grk3$^{-/-}$	Grk3^{tm1Rjl}	Kindly provided by Teresa Tarrant (Duke University, USA)
Grk5$^{fl/fl}$	Grk5^{tm2Rjl}	010960, Jackson Laboratories, Bar Harbor, ME
Grk6$^{fl/fl}$	Grk6^{tm1Mca}	010962, Jackson Laboratories, Bar Harbor, ME
Mrp8-Cre	Tg(S100A8-cre,-EGFP)1Ilw	021614, Jackson Laboratories, Bar Harbor, ME
Vav1-iCre	Commd10$^{Tg(Vav1-icre)A2Kio}$	008610, Jackson Laboratories, Bar Harbor, ME
Lyz2$^{gfp/+}$	Lyz2$^{tm1.1Graf}$	*Lyz2*^{gfp} were initially provided by Nicole Faust (Albert Einstein College of Medicine, NY)
Ly6g$^{cre/+}$	Ly6g$^{tm2621(cre,-tdTomato)Arte}$	Kindly provided by Matthias Gunzer (University Duisburg-Essen, Germany)
Rosa26$^{LSL:Tom}$	Gt(ROSA)26Sor$^{tm9(CAG-tdTomato)Hze}$	007905, Jackson Laboratories, Bar Harbor, ME
Lifeact-GFP	Tg(CAG-EGFP)#Rows	Kindly provided by Roland Wedlich-Söldner (University Münster, Germany)
CAG-DsRed	Tg(CAG-DsRed*MST)1Nagy/J	006051, Jackson Laboratories, Bar Harbor, ME
B6.Albino	Tyr^{c-2J}	000058, Jackson Laboratories, Bar Harbor, ME

These mouse strains were intercrossed to yield the following intercrosses: (a) *Mrp8-Cre*$^{+/-}$ *Grk2*$^{fl/fl}$, (b) *Mrp8-Cre*$^{+/-}$ *Grk2*$^{fl/fl}$ *Lifeact-GFP*$^{+/-}$, (c) *Vav-iCre*$^{+/-}$ *Grk2*$^{fl/fl}$, (d) *Mrp8-Cre*$^{+/-}$ *Grk5*$^{fl/fl}$, (e) *Mrp8-Cre*$^{+/-}$ *Grk6*$^{fl/fl}$, (f) *Mrp8-Cre*$^{+/-}$ *Grk2*$^{fl/fl}$ *Grk3*$^{-/-}$ *Grk5*$^{fl/fl}$ *Grk6*$^{fl/fl}$, (g) *Mrp8-Cre*$^{+/-}$ *Grk2*$^{fl/fl}$ *Lyz2*$^{gfp/+}$, (h) *Ly6g*$^{Cre/+}$ *Rosa26*$^{LSL:Tom}$ *Lyz2*$^{gfp/+}$, and (i) *Mrp8-Cre*$^{+/-}$ *Grk2*$^{fl/fl}$ *Rosa26*$^{LSL:Tom}$. Host for intradermal injections were *Tyr*$^{c-2J/c-2J}$ mice or *CAG-DsRed*$^{+/+}$ *Tyr*$^{c-2J/c-2J}$ mice, as indicated.

Table S2.

Table S2 lists the primers used for qRT-PCR

Gene	**Primers (forward; reverse)**
Grk2	5'-GGCCTGCTCACATCCCTTTT-3'; 5'-CTTCTGGAACACGTCCCCTC-3'
Grk3	5'-TATGGCTGCAGGAAAGCAGA-3'; 5'-AAAGGGACAATCCCCAGTGC-3'
Grk5	5'-GACCCCTTCCACGAGTACCT-3'; 5'-AGGCACAGACCTCTCCAAAG-3'
Grk6	5'-GTAGCGAACACGGTGCTACT-3'; 5'-GTCACGCTCAAGGCTGAGT-3'
18S rRNA	5'-GCAATTATTCCCCATGAACG-3'; 5'-GGCCTCACTAAACCATCCAA-3'
B2m	5'-CTGCTACGTAACACAGTTCCACC-3'; 5'-CATGATGCTTGATCACATGTCTCG-3'
Actb	5'-GGCTGTATTCCCCTCCATCG-3'; 5'-CCAGTTGGTAACAATGCCATGT-3'

Table S3.

Table S3 lists the statistical analysis used in each figure. Two-tailed *t* tests, paired *t* tests and analysis of variance (ANOVA) were performed after data were confirmed to fulfil the criteria of normal distribution and equal variance, otherwise two-tailed Kruskal–Wallis tests or Mann–Whitney *U* tests were applied. If overall ANOVA or Kruskal–Wallis tests were significant, we performed post hoc test with pair-wise comparisons (ANOVA: Tukey, Kruskal–Wallis: Dunn). Stars indicate significance (**P*≤0.05, ***P*≤0.01, ****P*≤0.001). Paired *t* tests for ratios were used when we assumed that a difference in the ratio is a consistent measure of the experimental effect, and pairing was part of the experimental design. NS indicates non-significant difference (*P*>0.05). Statistical analysis was performed using Prism software (GraphPad Software, Inc,Version 8.2.1 and 9.0.2).

Figure	**Statist. test**		**Post hoc test**	
1A	**ANOVA**	*F*=14.37, *DFn*=5, *Dfd*=12, *P*<0.001	**Tukey** WT:$Grk^{-/-}$ $Grk2^{-/-}$:4×$Grk^{-/-}$ WT:4×$Grk^{-/-}$	 ** (*P*≤0.01) NS (*P*>0.05) ** (*P*≤0.01)
1C *Speed* *y-Straightness*	 ***t* test** ***U* test**	 *t*=4.351, *df*=98, *P*<0.0001 *U*=757, *n*=50,50, *P*=0.0006		 *** (*P*≤0.001) *** (*P*≤0.001)
1D	***U* test**	*U*=0, *n*=50,50, *P*<0.0001		*** (*P*≤0.001)
1F *LTB4/CXCL2* *LTB4* *CXCL2* *FPR2* *FPR1* *C5a*	**One sample *t* test, theor. mean = 1**	 *t*=6,897, *df*=3, *P*=0.0062 *t*=4,859, *df*=3, *P*=0.0166 *t*=7,981, *df*=3, *P*=0.0041 *t*=3,916, *df*=3, *P*=0.0296 *t*=2,631, *df*=3, *P*=0.0783 *t*=2,958, *df*=3, *P*=0.0596		 ** (*P*≤0.01) * (*P*≤0.05) ** (*P*≤0.01) * (*P*≤0.05) NS (*P*>0.05) NS (*P*>0.05)
1G *LTB4/CXCL2* *LTB4* *CXCL2*	**Ratio paired *t* test**	 *t* ratio=9.355, df=3, *P*=0.0026 *t* ratio=6.808, df=3, *P*=0.0065 t ratio=19.54, df=3, *P*=0.0003		 ** (*P*≤0.01) ** (*P*≤0.01) *** (*P*≤0.001)
1H *LTB4 (2nd)* *LTB4 (3rd)*	 ***t* test** ***t* test**	 *t*=0.53, *df*=12, *P*=0.603 *t*=4.03, *df*=12, *P*=0.0017		 NS (*P*>0.05) ** (*P*≤0.01)
1I *CXCL2 (2nd)* *CXCL2 (3rd)*	 ***t* test** ***t* test**	 *t*=3.44, *df*=10, *P*=0.0063 *t*=3.99, *df*=10, *P*=0.0025		 ** (*P*≤0.01) ** (*P*≤0.01)
2B	***t* test**	*t*=6.06, *df*=58, *P*<0.0001		*** (*P*≤0.001)
2E *top*	***U* test**	*U*=1773, *n*=62,62, *P*=0.5536		NS (*P*>0.05)
2E *bottom*	**One sample *t* test, theor. mean = 1**	*t*=1.966, *df*=3, *P*=0.1440		NS (*P*>0.05)
2H	**ANOVA**	*F*=1.28, *DFn*=3, *Dfd*=15, *P*<0.001	**Tukey** $Grk2^{-/-}$:$Grk3^{-/-}$ $Grk2^{-/-}$:$Grk5^{-/-}$ $Grk2^{-/-}$:$Grk6^{-/-}$	 *** (*P*≤0.001) *** (*P*≤0.001) *** (*P*≤0.001)
2I	***t* test**	*t*=3.87, *df*=14, *P*=0.002		** (*P*≤0.01)
3D	**One sample *t* test, theor. mean = 1**	*t*=6.388, *df*=15, *P*<0.0001		*** (*P*≤0.001)

3E	***U* test**	U=739, n=59,48, P<0.0001		*** ($P \leq 0.001$)
3F	***U* test**	U=18, n=16,16, P<0.0001		*** ($P \leq 0.001$)
4C *left*	***U* test**	U=437, n=55,50, P<0.0001		*** ($P \leq 0.001$)
4C *right*	**Ratio paired *t* test**			
total 0 hours		t ratio=0.976, df=4, P=0.38		NS (P>0.05)
total 8 hours		t ratio=3.55, df=4, P=0.02		* ($P \leq 0.05$)
free 0 hours		t ratio=0.929, df=4, P=0.41		NS (P>0.05)
free 8 hours		t ratio=2.97, df=4, P=0.04		* ($P \leq 0.05$)
4E	***t* test**	t=3.85, df=6, P=0.008		** ($P \leq 0.01$)
4G	***U* test**	U=1401, n=74,74, P<0.0001		*** ($P \leq 0.001$)
4H	***U* test**	U=192, n=30,30, P<0.0001		*** ($P \leq 0.001$)
S1G				
LTB4/CXCL2	***U* test**	U=0, n=50,50, P<0.0001		*** ($P \leq 0.001$)
CXCL2	***U* test**	U=2, n=20,20, P<0.0001		*** ($P \leq 0.001$)
LTB4	***U* test**	U=7, n=18,18, P<0.0001		*** ($P \leq 0.001$)
S2A				
preNeu	***t* test**	t=0.42, df=8, P=0.68		NS (P>0.05)
immatureNeu	***t* test**	t=0.076, df=8, P=0.94		NS (P>0.05)
matureNeu	***t* test**	t=2.89; df=8, P=0.0202		* ($P \leq 0.05$)
S2B	***U* test**	U=8, n=5,5, P=0.42		NS (P>0.05)
S2E	**Ratio paired *t* test**			
WT:WT Inh		t=9.355, df=3, P=0.0026		** ($P \leq 0.01$)
Grk2$^{-/-}$:Grk2$^{-/-}$Inh		t=1.353, df=3, P=0.2690		NS (P>0.05)
S3A	**Ratio paired**			
pERK 50nM	***t* test**	t ratio=0.9937, df=2, P=0.4251		NS (P>0.05)
pERK 100nM		t ratio=3.053, df=2, P=0.0926		NS (P>0.05)
pERK 200nM		t ratio=4.544, df=2, P=0.0452		* ($P \leq 0.05$)
pERK triple		t ratio=5.244, df=2, P=0.0345		* ($P \leq 0.05$)
p-p38 50nM		t ratio=0.8697, df=2, P=0.4762		NS (P>0.05)
p-p38 100nM		t ratio=0.2787, df=2, P=0.8066		NS (P>0.05)
p-p38 200nM		t ratio=1.007, df=2, P=0.4198		NS (P>0.05)
p-p38 triple		t ratio=8.338, df=2, P=0.0141		* ($P \leq 0.05$)
S3B	**Ratio paired**			
pERK 50nM	***t* test**	t ratio=6.762, df=2, P=0.0212		* ($P \leq 0.05$)
pERK 100nM		t ratio=3.609, df=2, P=0.0690		NS (P>0.05)
pERK 200nM		t ratio=7.441, df=2, P=0.0176		* ($P \leq 0.05$)
pERK triple		t ratio=6.920, df=2, P=0.0203		* ($P \leq 0.05$)
p-p38 50nM		t ratio=5.239, df=2, P=0.0346		* ($P \leq 0.05$)
p-p38 100nM		t ratio=11.59, df=2, P=0.0074		** (P<0.01)
p-p38 200nM		t ratio=2.772, df=2, P=0.1092		NS (P>0.05)
p-p38 triple		t ratio=7.601, df=2, P=0.0169		* ($P \leq 0.05$)
S3C	**Ratio paired**			
pERK 5nM	***t* test**	t ratio=0.6921, df=2, P=0.5604		NS (P>0.05)
pERK 10nM		t ratio=0.8485, df=2, P=0.4855		NS (P>0.05)
pERK 20nM		t ratio=0.7944, df=2, P=0.5102		NS (P>0.05)
pERK triple		t ratio=0.3382, df=2, P=0.7674		NS (P>0.05)
p-p38 5nM		t ratio=3.952, df=2, P=0.0585		NS (P>0.05)
p-p38 10nM		t ratio=3.474, df=2, P=0.0738		NS (P>0.05)
p-p38 20nM		t ratio=2.840, df=2, P=0.1048		NS (P>0.05)
p-p38 triple		t ratio=3.126, df=2, P=0.0889		NS (P>0.05)
S3D	***t* test**	t=8.194, df=58, P<0.0001		*** ($P \leq 0.001$)
S3E	***t* test**	t=3.822, df=58, P=0.0003		*** ($P \leq 0.001$)

S3F	***t* test**	t=10.57, df=59, P<0.0001		*** ($P \leq 0.001$)
S4B	**ANOVA**	F=10.36, DFn=2, Dfd=87, P<0.0001	**Tukey** *Ctrl:MK886* *Ctrl:SB225002*	 *** ($P \leq 0.001$) *** ($P \leq 0.001$)
S5C *left*	***U* test**	U=1623, n=62,62, P=0.1361		NS (P>0.05)
S5C *right*	**One sample *t* test, theoretical mean = 1**	t=1.102, df=3, P=0.3509		NS (P>0.05)
S5E	***U* test**	U=0, n=4,5, P=0.016		* ($P \leq 0.05$)
S6A *0.1 µM* *1 µM*	 ***t* test** ***t* test**	 t=2.48, df=4, P=0.07 t=2.93, df=4, P=0.04		 NS (P>0.05) * ($P \leq 0.05$)
S6B *y-axis* *x-axis*	 **Kruskal–Wallis** **Kruskal–Wallis**	 H=133, n(group)=4, n(WT 1st,WT 2nd)= 344,156 , n(*Grk2*$^{-/-}$ 1st,*Grk2*$^{-/-}$ 2nd)= 396,820, P<0.0001 H=155, n(group)=4 , n(WT 1st,WT 2nd)= 344,156 , n(*Grk2*$^{-/-}$ 1st,*Grk2*$^{-/-}$ 2nd)= 396,820, P<0.0001	 **Dunn** *WT (1st:2nd)* *Grk2*$^{-/-}$ *(1st:2nd)* **Dunn** *WT (1st:2nd)* *Grk2*$^{-/-}$ *(1st:2nd)*	 *** ($P \leq 0.001$) * ($P \leq 0.05$) ** ($P \leq 0.01$) NS (P>0.05)
S6F	***U* test**	U=1915, n=80,80, P<0.0001		*** ($P \leq 0.001$)
S6G *infected* *control*	 ***U* test** ***U* test**	 U=49, n=10,10, P=0.97 U=11.5, n=5,5, P=0.89		 NS (P>0.05) NS (P>0.05)
S7F	***U* test**	U=442, n=38,75, P<0.0001		*** ($P \leq 0.001$)
S8A *unstimulated* *LTB4/CXCL2*	 ***t* test** ***t* test**	 t=0.12, df=8, P=0.91 t=0.69, df=8, P=0.51		 NS (P>0.05) NS (P>0.05)
S8B *unstimulated* *LTB4/CXCL2*	 ***t* test** ***t* test**	 t=0.0.9373, df=4, P=0.4017 t=0.1.885, df=4, P=0.1325		 NS (P>0.05) NS (P>0.05)
S8D	***U* test**	U=4, n=3,3, P>0.99		NS (P>0.05)
S8E	***U* test**	U=6, n=4,4, P=0.69		NS (P>0.05)
S8F *1 hour* *4 hours* *8 hours*	 ***U* test** ***U* test** ***U* test**	 U=7, n=4,4, P=0.89 U=8, n=4,4, P>0.99 U=7, n=4,4, P=0.89		 NS (P>0.05) NS (P>0.05) NS (P>0.05)

Table S4.

Table S4 lists the antibodies and dyes used for flow cytometry (FC) and immunoblot analysis (IB). Dilutions were made from the stock solutions of the company products.

	Clone	**Labeling**	**Company (Catalogue number)**	**Dilution**	**Assay**
Actin	polyclonal	–	Sigma-Aldrich (A2066)	1:1000	IB
GRK2	C-9	–	SCBT (sc-13143)	1:500	IB
Rabbit IgG		HRP	Dako (P0217)	1:6000	IB
Mouse IgG		HRP	Dako (P0161)	1:6000	IB
CD11b	M1/70	SB645	Invitrogen (64011282)	1:300	FC
CD16/CD32	2.4G2	–	BD Bioscience (553141)	1:200	FC
CD3e	145-2C11	PE-Cy7	Invitrogen (25003182)	1:1000	FC
CD45R/ B220	RA3-6B2	PE-Cy7	BioLegend (103221)	1:1000	FC
CD90.2 (Thy-1.2)	53-2.1	PE-Cy7	BioLegend (140309)	1:10000	FC
c-Kit	2B8	PE	Invitrogen (12117182)	1:800	FC
CXCR2	SA045E1	AF647	BioLegend (149603)	1:400	FC
CXCR4	2B11	biotin	Invitrogen (13999182)	1:200	FC
Fixable viability dye	–	eF506	ThermoFisher (65-0866-14)	1:1000	FC
Gr-1	RB6-8C5	PerCP-Cy5.5	Invitrogen (45593180)	1:3000	FC
LTB4R1	7A8	AF647 Labeling kit	AB: Merck (MABF2769) Labeling kit: Invitrogen (A20186)	1:35	FC
Ly-6G	1A8	APC-Cy7	BioLegend (127623)	1:300	FC
NK1.1	PK136	PE-Cy7	BioLegend (108713)	1:1600	FC
pospho-p38 MAPK (Thr180/Tyr182)	3D7	–	Cell Signaling (6908)	1:100	FC
pospho-p44/42 MAPK (Erk1/2) (Thr202/Tyr204)	197G2	AF647	Cell Signaling (13148S)	1:100	FC
Sca-1	D7	PE-Cy7	BioLegend (108113)	1:2000	FC
Siglec-F	E50-2440	PE-CF594	BD Bioscience (562757)	1:5000	FC
Streptavidin	–	BV421	BioLegend (405226)	1:200	FC